

Journal of Materials Chemistry B

Accepted Manuscript



This is an *Accepted Manuscript*, which has been through the Royal Society of Chemistry peer review process and has been accepted for publication.

Accepted Manuscripts are published online shortly after acceptance, before technical editing, formatting and proof reading. Using this free service, authors can make their results available to the community, in citable form, before we publish the edited article. We will replace this *Accepted Manuscript* with the edited and formatted *Advance Article* as soon as it is available.

You can find more information about *Accepted Manuscripts* in the [Information for Authors](#).

Please note that technical editing may introduce minor changes to the text and/or graphics, which may alter content. The journal's standard [Terms & Conditions](#) and the [Ethical guidelines](#) still apply. In no event shall the Royal Society of Chemistry be held responsible for any errors or omissions in this *Accepted Manuscript* or any consequences arising from the use of any information it contains.

Synthesis, Characterization, *In Vitro* Phantom Imaging, and Cytotoxicity of A Novel Graphene-Based Multimodal Magnetic Resonance Imaging - X-Ray Computed Tomography Contrast Agent

Gaurav Lalwani^{1†}, Joe Livingston Sundararaj^{2†}, Kenneth Schaefer^{1†}, Terry Button^{1,3} and Balaji Sitharaman^{1*}

¹Department of Biomedical Engineering, Stony Brook University, Stony Brook, New York
11794-5281

²Department of Materials Science and Engineering, Stony Brook University, Stony Brook, New
York 11794

³Department of Radiology, Stony Brook University, Stony Brook, New York 11794

[†]These authors contributed equally to the work.

*Correspondence:

Balaji Sitharaman, Ph.D.

Department of Biomedical Engineering

Bioengineering Building Room 115

Stony Brook University

Stony Brook, NY 11794-5281

Tel: 631-632-1810

Email: balaji.sitharaman@stonybrook.edu

Abstract:

Graphene nanoplatelets (GNPs), synthesized using potassium permanganate-based oxidation and exfoliation followed by reduction with hydroiodic acid (rGNP-HI), have intercalated manganese ions within the graphene sheets, and upon functionalization with iodine, show excellent potential as biomodal contrast agents for magnetic resonance imaging (MRI) and computed tomography (CT). Structural characterization of rGNP-HI nanoparticles with low- and high-resolution transmission electron microscope (TEM) showed disc-shaped nanoparticles (average diameter, 200 nm, average thickness, 3 nm). Energy dispersive X-ray spectroscopy (EDX) analysis confirmed the presence of intercalated manganese. Raman spectroscopy and X-ray diffraction (XRD) analysis of rGNP-HI confirmed the reduction of oxidized GNPs (O-GNPs), absence of molecular and physically adsorbed iodine, and the functionalization of graphene with iodine as polyiodide complexes (I_3^- and I_5^-). Manganese and iodine content were quantified as 5.1 ± 0.5 and 10.54 ± 0.87 wt% by inductively-coupled plasma optical emission spectroscopy and ion-selective electrode measurements, respectively. *In vitro* cytotoxicity analysis, using absorbance (LDH assay) and fluorescence (calcein AM) based assays, performed on NIH3T3 mouse fibroblasts and A498 human kidney epithelial cells, showed CD_{50} values of rGNP-HI between 179-301 $\mu\text{g/ml}$, depending on the cell line and the cytotoxicity assay. CT and MRI phantom imaging of rGNP-HI showed high CT (approximately 3200% greater than HI at equimolar iodine concentration) and MRI (approximately 59% greater than equimolar Mn^{2+} solution) contrast. These results open avenues for further *in vivo* safety and efficacy studies towards the development of carbon nanostructure-based multimodal MRI-CT contrast agents.

Introduction:

Magnetic resonance imaging (MRI) and X-ray computed tomography (CT) are two of the most widely used whole body imaging modalities in clinical radiology. Both these modalities have their strengths and weaknesses, with variable spatial and temporal resolution. To overcome their limitations, complementary use of both these modalities as a biomodal system significantly improves disease detection and diagnostic confidence.^{1 2, 3 4, 5} To achieve adequate contrast between diseased and normal tissue, numerous imaging procedures employ clinical MRI or CT contrast agents synthesized using the elements gadolinium and iodine, respectively. However, there are currently no clinically approved MRI-CT contrast agents. Thus, the development of multimodal MRI-CT contrast agents for systemic and targeted imaging remains an active area of research.⁶⁻⁸

There is a growing interest in developing nanoparticle-based contrast agents for multi-modal imaging with longer vascular half-life that would enable long term monitoring of the diseased tissues or organs.⁹⁻¹³ These nanoparticles have hybrid compositions synthesized using ceramics, polymers, or metals configured in various shapes (spheres, tubes, branched structures, and shells).^{5, 14, 15} For example, polymer coated Au-Fe nanoparticle conjugates,¹⁴ Ru(bpy):Gd³⁺/SiO₂ nanoparticles,¹⁶ and gadolinium-chelate coated gold nanoparticles,¹⁵ have been reported as potential multimodal MRI-CT contrast agents.

Carbon nanomaterials such as single-walled carbon nanotubes (SWCNTs), ultra-short carbon nanotubes (US-tubes), and fullerenes (C₆₀) encapsulating or embedding gadolinium have been

reported as contrast agents for either MR or CT imaging.¹⁷⁻²⁰ However, there are no reports on the development of multimodal MRI-CT contrast agents using these carbon nanomaterials. Recently, water-solubilized graphene nanoparticles, due to their unique nanoscopic properties, have demonstrated great potential for a variety of *in vivo* biomedical applications. Graphene nanoparticles (a.k.a. graphene nanoplatelets or GNPs) synthesized using the modified Hummer's method, or variations thereof,²¹ are used in most *in vitro* and *in vivo* biomedical studies, and are currently being investigated for a number of purposes such as drug / gene delivery agents,^{22, 23} tissue engineering,²⁴⁻²⁶ photothermal therapy,^{27, 28} as well as for bio-imaging applications.^{22, 29, 30} With the goal of developing novel carbon nanostructure-based high efficacy multimodal MRI-CT contrast agent, we here report on the synthesis, characterization, *in vitro* cytotoxicity, and phantom imaging of a novel GNP-based MRI-CT multimodal contrast agent.

Materials and Methods:

1. Synthesis

Oxidized GNPs (O-GNPs) were prepared using a variation of the modified Hummer's method, as described previously.³¹ Briefly, 2 g of pristine graphite flakes (Sigma Aldrich, NY, USA) were exfoliated with 98% formic acid (50 ml, Sigma Aldrich, NY, USA) in a round bottom flask and bath sonicated (FS-30, Fisher Scientific, NY, USA) for 2 hours at room temperature. The resulting micro-graphite particles were isolated by centrifugation (3000 rpm, 20 minutes), washed with DI water and acetone, and vacuum dried at 65°C overnight. Post vacuum drying, the graphite particles were mixed with nitric acid (20 ml, 69-70%, J. T. Baker, Phillipsburg, NJ, USA) on an ice bath and allowed to stir at 200 rpm. Ice-cold sulfuric acid (30 ml, 98%, J. T. Baker, Phillipsburg, NJ, USA) was added, followed by potassium permanganate (6 g, 99%, Sigma Aldrich, NY, USA). An ice bath was used to avoid sudden increases in the temperature of the round bottom flask. The mixture was subsequently maintained at 35°C in an oil bath for 2 hours under constant stirring. Next, 200 ml of DI water was added to the flask and the resulting brown colloidal suspension was stirred for an additional 30 minutes. The O-GNP suspension was subjected to centrifugation (3000 rpm, 20 minutes), and the resulting pellet was washed with DI water and hydrochloric acid (HCl, Sigma Aldrich, NY, USA). O-GNPs were isolated by centrifugation (4000 rpm, 1 hour), vacuum dried at 40°C overnight, and placed in a vacuum desiccator for 7 days.

Hydrazine-reduced GNPs (rGNP-N₂H₂) were synthesized from O-GNPs using a previously reported method.²¹ For HI based reduction; dried O-GNPs (200 mg) were suspended in 200 ml of DI water, and bath sonicated for 1 hour. A total of 1.5 ml of HI solution (32.1 mM, 99%, Sigma Aldrich, NY, USA) was added to the round bottom flask. The mixture was heated at 100°C in an oil bath under a water-cooled condenser for 24 hours. The rGNP-HI were isolated by centrifugation (3000 rpm, 20 minutes) and washed with DI water and methanol before being dried in a vacuum oven at 65°C overnight to obtain a dry powder.

2. Characterization

A. Electron microscopy and energy dispersive x-ray spectroscopy (EDX)

O-GNPs, rGNP-N₂H₂ and rGNP-HI (3 concentrations of HI) samples were suspended in 1:1 water:ethanol at a concentration of 1 mg/ml using bath sonication for 10 minutes. The resulting solutions were centrifuged at 5000 rpm for 5 minutes and spin coated (2000 rpm, 1 minute) on freshly cleaved silicon wafers (Ted Pella) for scanning electron microscopy (SEM). Solutions for transmission electron microscopy (TEM) were prepared by probe sonication (Cole Parmer Ultrasonicator LPX 750, 1 s “on”, 2 s “off”) and centrifugation at 5000 rpm for 5 minutes. The supernatants (10µl) were dropped on holey lacey carbon grids (300 mesh size, copper support, Ted Pella, USA) and dried overnight.

SEM was performed using LEO 1150 Gemini field emission scanning electron microscope (Department of Material Sciences, Stony Brook University, USA) at 20 kV using a Rutherford

backscattered and in-lens secondary electron detectors. High-resolution TEM was performed using a JOEL 2100F high-resolution analytical transmission electron microscope, equipped with EDX spectrometer, at the Center for Functional Nanomaterials (Brookhaven National Laboratories, NY, USA) at 200 kV. Low-resolution TEM imaging was performed using a FEI BioTwinG² transmission electron microscope (Central Microscopy Imaging Center, Stony Brook University, USA) at 80 kV.

B. Atomic Force Microscopy (AFM)

AFM imaging was performed using a modification of a previously described protocol.³² Briefly, nanomaterials were dispersed in 1:1 ethanol:water by probe sonication (Cole-Parmer Ultrasonicator LPX 750) for 30 seconds using a 1 s “on” and 2 s “off” cycle. 50 μ l of homogeneously dispersed nanomaterial solutions were dropped on freshly cleaved, isopropanol washed silicon wafers (Ted Pella, USA). Excess solutions were removed using blotting paper and the samples were air-dried. A NanoSurf EasyScan 2 Flex AFM (NanoScience Instruments Inc., Phoenix, AZ, USA), operating in tapping mode, using a V-shaped cantilever (APP Nano ACL – 10, W = 40 μ m, tip radius < 10 nm, frequency f_c = 145–230 kHz, L = 225 μ m, spring constant k = 20–95 N/m), was used for AFM imaging. To improve the nanomaterial density on the silicon wafer, 50 μ l of the nanomaterial solutions were dropped onto the same silicon wafer and the process was repeated.

C. Raman spectroscopy

WITec alpha300R Micro-Imaging Raman spectrometer was used for Raman analysis. Point spectra were recorded between 50-3750 cm^{-1} using a 532 nm Nd-YAG excitation laser at room temperature.

D. Elemental analysis

To determine manganese concentration in solid O-GNPs and rGNP-HI, inductively-coupled plasma optical emission spectroscopy (ICP-OES) was performed at micro-analytical analytical testing laboratories (Galbraith Laboratories, Inc., Knoxville, TN) on solid O-GNPs and rGNP-HI. Samples of known weight or concentration were treated with concentrated HNO_3 , heated to obtain a solid residue, treated with 30% H_2O_2 , and heated again to remove any carbonaceous material. For the ICP-OES analysis, the residue was dissolved in 2% HNO_3 before measurement.

To determine the iodine concentration in the rGNP-HI samples, ion selective electrode measurements were performed at Galbraith Laboratories Inc. (Knoxville, TN, USA) using an iodide specific electrode coupled with a pH meter. Samples were prepared using a commonly used oxygen combustion method for detection of halogens.³³ Briefly, rGNP-HIs (35-40 mg) were added to the combustion flask, purged with oxygen, ignited, and sealed immediately. Once the combustion was complete, the flask was inverted several times for effective absorption of iodine gas. Iodine quantification was performed according to American Society for Testing and Materials (ASTM) standard ASTM E-442 (test method for chlorine, bromine, or iodine in organic compounds by oxygen flask combustion).

E. X-ray diffraction analysis (XRD)

XRD analysis was performed on a Philips Analytical X-ray detector in the Department of Materials Science and Engineering, Stony Brook University. Dry powder samples were pressed on the sample holder (rectangular cavity, 1.5 cm x 1.5 cm x 0.05 cm). XPLOT was used for the manipulation of X-ray diffraction patterns. Diffraction peaks were located and compared to the reference peaks using the ICDD database. PC-1710 and Powder-X softwares were used to background subtraction, smoothing operation and acquisition of diffraction patterns.

3. Cytotoxicity

A. Lactate dehydrogenase assay

The membrane integrity of cells as a measure of cell death was evaluated by quantifying the amount of lactate dehydrogenase (LDH, TOX-7 LDH Kit, Sigma Aldrich, NY, USA) released in the media after 24 and 48 hours of exposure to rGNP-HI. NIH3T3 and A498 cells were plated in a 96-well plate at a density of 5×10^4 cells per well. Dried powdered rGNP-HI was weighed and dispersed in DSPE-PEG (1,2-distearoyl-sn-glycero-3-phosphoethanolamine-N-[amino(polyethylene glycol)]) solution (1.2 mg/ml of DSPE-PEG in DI water). Before commencing the assay, the media from each well were replaced with 180 μ l of fresh media. Stock solutions of rGNP-HI (20 μ l) at various concentrations were prepared and added to the wells for final treatment concentrations of 10, 100, 250, and 500 μ g/ml. The cells were incubated at 37°C for 24 and 48 hours. After each time point, the media were removed from the individual wells and centrifuged at 1200 rpm for 5 minutes. From each well, 50 μ l of the media supernatants were collected and transferred to a fresh 96 well plate. A total of 100 μ l of LDH assay mixture was added to each well, followed by incubation in the dark for 30 minutes. 1N

HCl (10% volume) was added to each well to stop the assay, and absorbance values were recorded at 490 nm. Cells for positive control (100% dead) were incubated with 20 μ l of lysis solution for 45 minutes before centrifugation. Cells cultured on tissue culture polystyrene (TCPS) served as the baseline control. The LDH release (% of positive control) was expressed as the percentage of $(OD_{\text{test}} - OD_{\text{blank}})/(OD_{\text{positive}} - OD_{\text{blank}})$, where OD_{test} is the optical density of the baseline control cells or cells exposed to rGNP-HI, OD_{blank} is the optical density of the wells without cells, and OD_{positive} is the optical density of the positive control cells. Absorbance of culture media containing DSPE-PEG was measured for baseline correction, and LDH release from cells upon incubation with DSPE-PEG was also measured (Tecan Infinite M200 96 well plate reader, Zurich, Switzerland).

B. Calcein-AM (LIVE) assay

The calcein-AM (calcein acetoxymethyl ester) assay was used to determine the viability of cells. Calcein-AM is converted to green fluorescent calcein upon hydrolysis by esterases present inside living cells, and the fluorescent intensity is directly proportional to the amount of live cells. A fluorescent microplate reader protocol, used according to the manufacturer's instructions. (LIVE/DEAD® viability/cytotoxicity kit for mammalian cells, Cat. No. L-3224, Invitrogen Molecular Probes, OR, USA) was used for this assay. Similar to the LDH assay, NIH3T3 cells and A498 cells were plated at a density of 5×10^4 cells per well in a 96-well plate and incubated with rGNP-HI at various concentrations (10-500 μ g/ml) for 24 and 48 hours. After each time point, media were removed from the wells and the cells were washed with PBS (3x). Calcein-AM solution (100 μ l) was added to each well, and the wells were incubated for 30 minutes. Absorbance values were recorded using a 96-well plate reader (Tecan Infinite M200, Zurich,

Switzerland) at excitation/emission wavelengths of 490/530 nm. Cells cultured on TCPS were used as positive controls. For negative control, cells treated with lysis buffer 45 minutes prior to staining were used. The percentages of live cells (w.r.t. TCPS controls) were calculated from the fluorescence readings as follows:

$$\% \text{ Live Cells} = \frac{[F(530)_{\text{sam}} - F(530)_{\text{min}}]}{[F(530)_{\text{max}} - F(530)_{\text{min}}]} \times 100$$

where $F(530)_{\text{sam}}$ is the fluorescence of cells labeled with calcein-AM at 530 nm in the experimental group, $F(530)_{\text{max}}$ is the fluorescence of wells where all (or nearly all) cells are alive i.e. the positive control (TCPS group) labeled with calcein-AM, $F(530)_{\text{min}}$ is the fluorescence of wells where all (or nearly all) cells are dead and labeled with ethidium homodimer-1 (EthD-1). Fluorescence readings were recorded of cell-free wells containing media in the presence of calcein-AM as the background and subtracted from all values of $F(530)$ before calculation of the results. For fluorescence imaging, NIH3T3 cells were seeded in 35 mm tissue culture polystyrene plates at a density of 50,000 cells per plate. Cells were exposed to rGNP-HI at concentrations ranging 1-50 $\mu\text{g/ml}$ for 48 hours, washed, and stained with calcein-AM and EthD-1. Imaging was performed using a Zeiss 1016-758 fluorescence microscope equipped with AxioCam MRc, and AxioVision 4.7.2 software.

4. Phantom Imaging

A. Computed tomography

Computed tomography (CT) phantom imaging was performed on graphene samples using a GE 64 slice Lightspeed VCT CT scanner to determine radiodensity (Cancer Center, Stony Brook University, NY, USA). Samples were prepared by dispersing graphene powder in DI water (43

mg/ml). The CT scanner, operated at 80 kV and 120 kV (section thickness = 5), exposed a head phantom consisting of rGNP-HI (43 mg/ml), HI in DI water, manganese chloride (MnCl_2 solution), and DI water. The concentration of manganese and iodine in these control samples were equimolar to the concentrations of these elements in rGNP-HI.

B. Magnetic resonance imaging

T_1 weighted magnetic resonance (MRI) phantom imaging was performed using a 1.5 T clinical GE scanner (Stony Brook University Hospital, Stony Brook, NY) on the same samples used for CT phantom imaging. The repetition time (TR) and echo time (TE) were set at 800 ms and 10 ms, respectively. The flip angle was 90° and the field of view was 100 x 100 mm. The in-plane resolution was 2.56 pixel/mm, and slice thickness was set to 3 mm.

5. Cell Culture

National Institutes of Health mouse fibroblasts (NIH3T3 cells) and human kidney epithelial cells (A498 cells) were used to assess the cytotoxicity of rGNP-HI. Both cell lines were obtained from ATCC (Manassas, VA, USA). NIH3T3 cells were grown in Dulbecco's Modified Eagle Medium (DMEM), and A498 cells were grown in Eagle's Minimum Essential Medium (EMEM), both which were supplemented with 10% fetal bovine serum (FBS) and 1% penicillin-streptomycin. Media were changed twice a week, and the cells were maintained at 37°C in a 95% O_2 - 5% CO_2 environment.

6. Statistical Analysis

All data are represented as means \pm SD for $n=6$ samples. A 95% confidence interval was used for all statistical analyses ($p < 0.05$). One-way ANOVA followed by Tukey-Kramer post hoc analyses were used for multiple comparisons between groups.

Results and Discussions

We here investigated the differences between rGNP-HI (O-GNPs reduced with hydrogen iodide (HI, 8.02 mM)) compared to O-GNPs and O-GNPs reduced with hydrazine hydrate (N_2H_2 , 32.1 mM) (controls). High-resolution TEM (HRTEM) and SEM (HRSEM) were performed for the structural characterization of rGNP-HI. Figure 1A, B (HRTEM) and C (low-resolution TEM) shows the characteristic disc-shaped morphology (diameter \approx 200 nm) of rGNP-HI. AFM topography imaging (Figure 1D) further corroborated the diameter distribution of rGNP-HI, as determined by analyzing multiple TEM images ($n=10$). The thickness of rGNP-HI was approximately 2-5 nm (Figure 1E, AFM height profile), corresponding to roughly 5-15 layers of graphene (calculated assuming the thickness of single layer graphene = 0.34 nm).²⁴ The presence of iodine and manganese in rGNP-HI was detected by HRTEM-EDX (Figure 1F). Figure 1G-I shows SEM images of O-GNPs, rGNP- N_2H_2 and r-GNP-HI with the corresponding EDX spectra. The SEM-EDX spectra of O-GNPs showed peaks for oxygen (O) at 0.52 KeV, and manganese (Mn) at 5.9 KeV. Additionally, a minor peak for potassium (K), and trace amounts of silicon (Si) and copper (Cu) were also detected. For rGNP- N_2H_2 , reduction in the intensity of the (O) peak was observed, and implied removal of oxygen from the graphitic structure (Figure 1H). Similarly, the r-GNP-HI sample showed trace amounts of oxygen, indicating the reduction of O-GNPs using HI (Figure 1I). In addition to a minor peak for manganese, a sharp peak was observed at 3.94 KeV, which was attributed to the presence of iodide (I).

Raman spectroscopy has been extensively used for the structural characterization of carbon nanomaterials.^{34, 35} Figure 2 displays the Raman spectra of O-GNPs, rGNP-N₂H₂ and rGNP-HI, together with the spectrum of pristine graphite powder for comparative purposes. Raman peaks at 1335 cm⁻¹ (D band), 1565 cm⁻¹ (G band), and 2680 cm⁻¹ (2D band) were observed for pristine graphite, whereas Raman peaks at 1357 cm⁻¹ and 1594 cm⁻¹ were observed for O-GNPs. A sharp increase in the ratio of the intensity of D to G peaks (I_D/I_G) was observed, indicating the disruption of the sp² bonding of pristine graphene. Additionally, for O-GNPs, higher frequency shifts in the D band (22 cm⁻¹) and G band (29 cm⁻¹) were also observed.³⁶ The I_D/I_G ratio for pristine graphite was 0.28, which increased to 0.96 upon oxidation. The Raman spectrum of rGNP-N₂H₂ exhibited peaks at 1339 cm⁻¹ and 1593 cm⁻¹. For rGNP-HI, in addition to D and G bands at 1343 cm⁻¹ and 1584 cm⁻¹, two additional peaks at 117 cm⁻¹ and 154 cm⁻¹, denoting the presence of polyiodides (I₃⁻ and I₅⁻), were observed.^{17, 37, 38} Moreover, a peak at 181 cm⁻¹ corresponding to molecular iodine was absent, negating the possibility of physical accumulation of iodine on graphene sheets.³⁷ The I_D/I_G ratio after reduction increased to 1.07 for rGNP-N₂H₂ and 1.01 for rGNP-HI, which can be attributed to the reduction in the average size of sp² domains in addition to an increase in the number of these small disorder domains.^{21, 39}

The X-ray diffraction spectra for pristine graphite, O-GNPs, and rGNP-HI are presented in Figure 3. Pristine graphite shows a characteristic peak at $2\theta = 26.6^\circ$ ($d \sim 3.34 \text{ \AA}$, 002 peak). The XRD spectrum of O-GNPs shows peaks at $2\theta = 26.6^\circ$, 42.8° , and 44.9° , attributed to the presence of graphite (possibly due to incomplete oxidation), and three-dimensional stacks of turbostratic graphene, as reported previously.⁴⁰⁻⁴² rGNP-HI showed peaks at $2\theta = 24.4^\circ$ and 26.5° , attributed to reduced graphene, and at $2\theta = 43^\circ$ and 44.7° , which corresponded to

turbostratic graphene.⁴² Additionally, peaks observed at 38.68° and 44.7° may correspond to the presence of aluminum as a trace impurity in the sample.⁴³ However, absence of a peak at $2\theta = 19.6^\circ$ was indicative of no adsorption of hexagonally packed I_2 molecules, and implies the presence of iodine as polyiodides in the graphene sheet, corroborating the Raman spectroscopy findings (Figure 2).⁴⁴ Furthermore, in comparison to graphite, broadening of peaks in the XRD spectrum for rGNP-HI and O-GNPs was observed, suggesting a step-by-step loss of crystallinity of graphene upon oxidation and subsequent reduction.^{41, 42}

Iodine in its ionic form (I^-) in aqueous solution can be determined potentiometrically using an iodide specific electrode coupled with a pH meter. This method can measure total elemental iodine along with iodates (IO_3^- , IO_5^- , after their reduction to I^- by hydrazine) when used in conjunction with oxygen flask combustion.³³ The concentration of iodide in unknown samples can be determined by comparison to a linear regression analysis of known reference standards (lower limit of quantitation = 0.01 mg/l). Ion selective electrode measurements confirmed the presence of iodine in rGNP-HI. The iodine content in rGNP-HI (reduced by 32.1mM HI) was quantified as $10.54 \pm 0.87\%$ (mean \pm SD for three batches of rGNP-HI). Our analysis also indicated that increases in the concentration of HI lead to better reduction of graphene oxide, while simultaneously increasing the iodine content in the GNPs (Figure 1J). We have previously used inductively-coupled plasma optical emission spectroscopy (ICP-OES) to quantify the amount of manganese present in oxidized and reduced GNPs.³¹ The amount of manganese present in oxidized and reduced graphene nanoplatelets was 4.5 ± 0.4 wt% and 5.1 ± 0.5 wt%, respectively.

Evaluation of the cytocompatibility is the first step towards the development of any new material for biomedical applications. Several studies have reported that toxicity and cellular responses vary depending on the structure of the carbon nanomaterial, dispersion state, chemical functionalization, and method of synthesis.^{20, 45-48} Therefore, the cytotoxicity of every new carbon nanomaterial must be evaluated individually as a different compound. Here, we analyzed the cytotoxicity of rGNP-HI using concentrations ranging from 10 - 500 $\mu\text{g/ml}$ and using two cell lines (NIH3T3 fibroblast cells and human kidney epithelial A498 cells) at two different time points (24 and 48 hours). NIH3T3 fibroblast cells were chosen since they have been widely used previously for *in vitro* cytotoxicity screening of several nanoparticle formulations.^{20, 49} Similar to other carbon nanostructure-based contrast agents,²⁰ intravenously injected rGNP-HI formulations will be primarily excreted by the renal route, and several reports have highlighted the nephrotoxicity of iodine or gadolinium-based CT or MRI contrast agents.^{50, 51} Thus, in addition to NIH3T3 cells, cytotoxicity assessment of DSPE-PEG dispersed rGNP-HI solutions was also performed using A498 human kidney epithelial cells. One of the most commonly used method for the cytotoxicity evaluation of nanomaterials – MTT assay – has been reported to generate erroneous results in case of carbon nanomaterials due to interactions between carbon nanomaterials and insoluble formazan crystals.⁵² Furthermore, due to several contradictory reports on the cytotoxicity of carbon nanomaterials, it is recommended to use at least two cytotoxicity assays for confident measurements.⁵² Therefore, in this study, we have employed two independent assays - LDH assay and calcein-AM LIVE assay, to assess the cytotoxicity of rGNP-HI.

The LDH assay has been widely used to assess *in-vitro* cytotoxicity of graphene-based nanostructures.⁴⁶ This assay measures the amount of the cytosolic enzyme lactate dehydrogenase (LDH) released by apoptotic or necrotic cells in the culture media. LDH present in the culture media catalyzes the oxidation of lactate to pyruvate and reduction of NAD⁺ to NADH. The newly formed NADH subsequently catalyzes the conversion of iodonitrotetrazolium (INT) to a colored, water-soluble formazan product with a strong absorbance at 490 nm. Figure 4A and B show the LDH release (%) from NIH3T3 and A498 cells after 24 and 48 hours of exposure to rGNP-HI at various concentrations. The CD₅₀ values of DSPE-PEG dispersed rGNP-HI solutions for NIH3T3 and A498 cells, as determined by the LDH assay, are reported in Table 1. For NIH3T3 and A498 cells, no significant differences in the % LDH release between baseline control and DSPE-PEG groups were observed, suggesting that DSPE-PEG at concentrations used for the dispersion of rGNP-HI does not induce cell death. At the highest concentration (500 µg/ml), NIH3T3 cells showed a maximum LDH release of approximately 55% and 60% at the 24- and 48-hour time points, respectively, compared to the positive control (lysed cells). A significant increase in the % LDH release for NIH3T3 cells (compared to baseline control) at both time points were observed after treatment with 100 µg/ml DSPE-PEG dispersed rGNP-HI solution. Similar to NIH3T3 cells, A498 cells showed a maximum cell death of approximately 55% and 60% at 24 and 48 hours, respectively, at the highest treatment concentration. Furthermore, A498 cells, at both 24 and 48 hours, showed higher % LDH release compared to the baseline control at the 250 µg/ml treatment concentration. The % LDH release at treatment concentrations below 100 µg/ml was similar to, or slightly lower than, the baseline controls for both NIH3T3 and A498 cells at both time points, suggesting that rGNP-HI at concentrations below 100 µg/ml do not induce cell death.

Calcein AM is a non-fluorescent, cell-permeable dye, widely used to determine cell viability of eukaryotic cells.⁴⁸ Upon cellular internalization, the acetoxymethyl ester group of calcein AM is hydrolyzed by intracellular esterases, forming calcein, a green fluorescent dye retained in the cytoplasm. Figure 4C and D show the % cell viability (normalized to TCPS controls) of NIH3T3 and A498 cells at various treatment concentrations (10–500 $\mu\text{g/ml}$) of rGNP-HI. The CD_{50} values of DSPE-PEG dispersed rGNP-HI solutions against NIH3T3 and A498 cells determined by calcein AM fluorescence-based assay are reported in Table 1. For both NIH3T3 and A498 cells, no significant differences in the % cell viability between baseline control (cells cultured on TCPS in the absence of exposure to rGNP-HI) and DSPE-PEG groups were observed for both time points. Significant decreases in the % cell viability for NIH3T3 cells (compared to baseline control) at both time points were observed at the 100 $\mu\text{g/ml}$ treatment concentration. Similar to NIH3T3 cells, A498 cells showed a minimum cell viability of approximately 30% at 24 and 48 hours upon exposure to the highest treatment concentration. Furthermore, A498 cells showed significantly lower cell viability after treatment with 100 $\mu\text{g/ml}$ rGNP-HI at both 24 and 48 hours. The cell viability at treatment concentrations < 100 $\mu\text{g/ml}$ was similar to, or slightly lower than, the baseline controls for NIH3T3 and A498 cells at both time points.

The LIVE/DEAD viability/cytotoxicity assay uses two-color fluorescence—green fluorescence from calcein dye (marker of live cells) and red fluorescence from EthD-1 (marker of dead cells). Generally, therapeutic doses of drug formulations are 5-10 times lower than LD_{50} or CD_{50} values. Therefore, cells were treated with rGNP-HI concentrations ranging from 1-50 $\mu\text{g/ml}$.

Figure 4 (E) shows representative fluorescence images of NIH3T3 cells stained with calcein-AM and EthD-1 after 48 hours of exposure to rGNP-HI at concentrations of 1 $\mu\text{g/ml}$ [(c) & (d)], 10 $\mu\text{g/ml}$ [(e) & (f)], 25 $\mu\text{g/ml}$ [(g) & (h)] and 50 $\mu\text{g/ml}$ [(i) & (j)]. Images (a) & (b) are control cells (no exposure). A dose dependent increase in cell death can be observed. However, the number of dead cells is significantly lower than live cells for every treatment concentration.

Taken together, the results of the LDH assay, calcein-AM assay, and LIVE/DEAD fluorescence imaging showed an increase in the cell death of NIH3T3 and A498 cells with increasing concentrations of rGNP-HI. However, the viability values from both LDH and calcein-AM assays cannot be compared directly due to variations in the sensitivity of these assays attributable to differences in their detection methods. After 24 and 48 hours, at treatment concentrations below 100 $\mu\text{g/ml}$, the viability of both the cell lines was comparable to baseline controls, and several studies have reported that graphene nanoparticles at concentrations below 50 $\mu\text{g/ml}$ are relatively safe for various cell types.^{45, 46, 48} The CD_{50} values of graphene nanoparticles vary significantly depending on several parameters such as method of synthesis, dispersion state, size, morphology, chemical functionalization, and the cell types under investigation.⁴⁶⁻⁴⁸ The viability results of this study suggest that rGNP-HI dispersed in DSPE-PEG at concentrations < 179 $\mu\text{g/ml}$ (CD_{50} : range, 179-301 $\mu\text{g/ml}$) represent potentially safe doses for future *in vitro* and *in vivo* safety and efficacy studies.

CT and MRI phantom imaging were performed on aqueous dispersions of rGNP-HI to assess their potential as dual CT-MRI contrast agents. rGNP-HI were dispersed at a concentration of 43

mg/ml in DI water. As controls, DI water, manganese chloride (MnCl_2) solution, and HI were also imaged. The manganese concentration in MnCl_2 (39.8 mM) and iodine concentration in HI (32.1 mM) were equimolar to the concentration of these elements in rGNP-HI. Figure 5A shows the CT phantom images obtained using a clinical CT at 80 and 120 kV X-ray potential. rGNP-HI showed significant greater CT contrast compared to the control solutions. Setting the radiodensity of air to -1000 HU (Hounsfield Units) and water to 0 HU, the radiodensity of rGNP-HI was calculated to be 1980 HU, which is approximately 10 times greater than the currently used CT contrast agents such as Omnipaque.⁵³ The iodine content in rGNP-HI was approximately 10% (as determined by ICP analysis), and therefore, the iodine concentration in 43 mg/ml rGNP-HI dispersion used for CT phantom imaging was calculated to be approximately 33.8 mM. For comparative purposes, the CT numbers for Omnipaque at 40 mM iodine concentration is approximately 175,⁵³ and a 5 mg/ml phantom of pure iodine solution is approximately 100.⁵⁴ Manganese (determined as 5.1 wt% for reduced graphene nanoplatelets; manganese has an x-ray absorption coefficient of $0.33 \text{ cm}^2 \text{ g}^{-1}$ at 100 KeV) could potentially also be contributing to the x-ray absorption of rGNP-HI. Figure 5B shows the T_1 -weighted phantom images, obtained using a 1.5 Tesla clinical MRI system for rGNP-HI, MnCl_2 and HI acid. Pixel intensity values for MRI phantoms were determined by image processing using ImageJ (National Institutes of Health, Bethesda, MD, USA). In comparison to the background (no contrast agent, pixel intensity = 0), the mean pixel intensity values were approximately 330%, 703%, and 1120% higher for HI acid, MnCl_2 , and rGNP-HI, respectively. The T_1 relaxation times were 959, 364, and 260 ms for HI acid, MnCl_2 , and rGNP-HI, respectively.

Rivera and coworkers have recently reported the use of US-tubes (Bi@US-tubes) as a potential X-ray imaging contrast agent.⁵⁵ Their phantom imaging studies illustrated that the CT coefficient value of Bi@US-tubes suspensions in Pluronic® F-108 NF was 1079 HU per mM, which is higher than the radiodensity of rGNP-HI. However, the results of our study cannot be directly compared to theirs, due to differences in the morphology of carbon nanostructures (graphene vs. US-tubes) and radio-opaque elements (iodine, manganese vs. bismuth). X-ray beam attenuation depends on beam energy and the density of body tissues. For example; kidneys, muscles, liver and soft tissue tumors exhibit attenuation between 30-60 HU, body fluids between 0-30 HU, and body fat exhibits attenuation between -130 to -70 HU.⁵⁶ For an X-ray imaging contrast agent, a minimum detectable difference of 30 HU is considered necessary to distinguish tissue abnormalities (such as tumors) from the neighboring healthy tissues.⁵⁶ Due to the high CT number of rGNP-HI, this criterion can be satisfied at relatively low concentrations below 1 mg/ml of rGNP-HI. Moreover, the radiodensity value of rGNP-HI reported in this study was significantly greater (2-55 times) than other CT contrast agents such as inorganic nanoparticles (gold-iron oxide polymeric conjugates,¹⁴ iron-platinum nanoparticle conjugates,⁵ polymer coated bismuth nanoparticles⁵⁷) and iodine encapsulating carbon nanoparticles (I₂@SWCNTs, I₂@US-tubes and I₂@C₆₀).²⁰

Over the last decade, several gadolinium carbon nanostructures complexes have been reported as potential high performance MRI contrast agents.^{18, 20, 58, 59} Recently, FDA has restricted the use of Gd³⁺ based MRI contrast agents in patients suffering from renal insufficiency (glomerular filtration rate < 30 ml/min/1.73 m²) due to the increased risk of nephrogenic systemic fibrosis associated with these agents. Manganese is a natural constituent of cellular metabolic pathways

(cofactor for receptors and enzymes). As a result, researchers have refocused their efforts on the development of manganese-based MRI contrast agents.⁶⁰ Previous reports show that Mn^{2+} intercalated GNPs exhibit high r_1 relaxivity (upto $92 \text{ mM}^{-1}\text{s}^{-1}$; an order of magnitude greater than the r_1 relaxivity values of FDA-approved Gd^{3+} and Mn^{2+} chelate-based T_1 MRI contrast agents ($2.2\text{--}4.5 \text{ mM}^{-1}\text{s}^{-1}$)).^{30, 31, 61} Relaxometry studies also indicate that multiple structural and molecular dynamic parameters (such as hydration number, rotational correlation time), that characterize interactions between water molecule and graphene, can be modulated.³¹ These parameters affect the T_1 relaxation mechanism. The size distribution of GNPs and other macromolecular contrast agents is similar,³⁰ suggesting that GNPs may possess extended intravascular residence time, and may be suitable as blood-pool contrast agents. Future *in vivo* studies will provide insights into its potential applications as an MRI-CT contrast agent.

Prolonged exposure to high concentrations of manganese can cause adverse health effects such as cardiac dysfunction and manganism (Parkinson-like neurological disorder).⁶⁰ Elevated physiological levels of iodine can result in thyroid diseases and nephrotoxicity.⁵⁰ Therefore, it is important to determine the physiological stability of manganese and iodine present in rGNP-HI. Several recent reports have documented that oxidized GNPs synthesized using potassium permanganate-based oxidative methods leads to robust confinement (intercalation) of trace amounts (ppm levels) Mn^{2+} ions between the graphene sheets.^{30, 31, 62, 63} We previously used the sodium bismuthate (NaBiO_3) test to determine the propensity of the intercalated Mn^{2+} ions to dissociate within 24 h. Those results showed no dissociation of Mn^{2+} ions in physiological fluids and biological buffers at least short term (24h).^{30, 31} Raman spectroscopic analysis (Figure 2) of rGNP-HI confirmed the absence of physically adsorbed iodine, and the presence of iodine as

polyiodide complexes covalently functionalized on the graphene sheets.³⁸ Taken together, these results suggest that these elements should not dissociate immediately under physiological conditions. However, a firm conclusion can only be drawn after additional *in vitro* long-term (24 hours) and *in vivo* thermal stability studies of rGNP-HI are completed.

Reduction of oxidized graphene using various methods such as chemical (treatment with hydrazine hydrate, sodium borohydrate) and thermal (annealing at high temperature) have been successfully used to restore the structural, electronic, and thermal properties of graphene.⁶⁴ Recent studies suggest that, in comparison to hydrazine and other reducing agents, HI could lead to better/equivalent reduction of graphene oxide.⁶⁵ Our results support these other findings, and provide additional thorough and integrated analyses of the structural and chemical properties of HI-reduced GNPs. Our results demonstrate that HI-based reduction of graphene oxide leads to the functionalization of graphene with iodine in the form of polyiodide complexes (I_3^- and I_5^-). rGNP-HIs are cyto-compatible (CD_{50} values between 179-301 $\mu\text{g/ml}$ depending on the cell line and type of cytotoxicity assay) and show excellent potential for the use as biomodal contrast agents for MRI and CT imaging.

To the best of our knowledge, this is the first report on a potential carbon nanostructure-based multimodal MRI-CT contrast agent. While previous studies have reported the potential of polymer-coated Au-Fe nanoparticle conjugates,¹⁴ Ru(bpy):Gd³⁺/SiO₂ nanoparticles,¹⁶ and gadolinium-chelate coated gold nanoparticles¹⁵ as multimodal MRI-CT contrast agents, the use of graphene towards the design of multimodal MRI-CT contrast agents offers several advantages

over these existing conjugates, including: (1) compared to CNTs and other gadolinium conjugated nanoparticle-based contrast agents, graphene, which is a 2-D sheet of carbon atoms, possesses a high surface area and can be easily dispersed in several biological solvents. Preparation of stable colloidal dispersions of graphene sheets in water is an important requirement towards their use for *in vivo* bio-imaging applications. (2) Graphene sheets possess sp^2 bonded carbon atoms that can be directly functionalized to improve dispersion and impart site-specific targeting capabilities, which is important for drug delivery applications (3) Graphene nanostructures can be developed as theragnostic agents, enabling simultaneous diagnosis using MRI-CT, and therapy by near infrared-induced hyperthermia.

Conclusion:

In conclusion, the reduction of graphene nanoplatelets (containing intercalated Mn^{2+} , synthesized using potassium permanganate-based oxidation and exfoliation) by hydroiodic acid leads to the functionalization of graphene sheets with iodine (polyiodide complexes: I_3^- and I_5^-). *In vitro* cytotoxicity analyses, using absorbance (LDH assay) and fluorescence (calcein AM) based assays, performed on NIH3T3 mouse fibroblasts and A498 human kidney epithelial cells, showed that rGNP-HI are cytocompatible ($\text{CD}_{50} \approx 179\text{-}301 \mu\text{g/ml}$). CT and MRI phantom imaging of rGNP-HI showed high CT (radiodensity of rGNP-HI was 1980 HU; approximately 3200% greater than HI at equimolar iodine concentration) and MRI (approximately 59% greater than equimolar Mn^{2+} solution) contrast. The promising CT and MRI contrast, in conjunction with the potentially low cytotoxicity of rGNP-HI reported herein open avenues for further *in vivo* safety and efficacy studies towards the development of carbon nanostructure-based multimodal MRI-CT contrast agent.

Acknowledgements:

This work was supported by the National Institutes of Health (Grant No. 1DP2OD007394-01).

We thank Ms. Cecilia Petrus for language editing and proofreading of the manuscript.

References:

1. Liebeskind, D. S.; Alexandrov, A. V., Advanced multimodal CT/MRI approaches to hyperacute stroke diagnosis, treatment, and monitoring. *Ann N Y Acad Sci* **2012**, 1268, 1-7.
2. Rosenman, J. G.; Miller, E. P.; Tracton, G.; Cullip, T. J., Image registration: an essential part of radiation therapy treatment planning. *Int J Radiat Oncol Biol Phys* **1998**, 40, (1), 197-205.
3. Rasch, C.; Barillot, I.; Remeijer, P.; Touw, A.; van Herk, M.; Lebesque, J. V., Definition of the prostate in CT and MRI: a multi-observer study. *Int J Radiat Oncol Biol Phys* **1999**, 43, (1), 57-66.
4. Zheng, J.; Perkins, G.; Kirilova, A.; Allen, C.; Jaffray, D. A., Multimodal contrast agent for combined computed tomography and magnetic resonance imaging applications. *Invest Radiol* **2006**, 41, (3), 339-48.
5. Chou, S. W.; Shau, Y. H.; Wu, P. C.; Yang, Y. S.; Shieh, D. B.; Chen, C. C., In vitro and in vivo studies of FePt nanoparticles for dual modal CT/MRI molecular imaging. *J Am Chem Soc* **2010**, 132, (38), 13270-8.
6. Mahmoudi, M.; Serpooshan, V.; Laurent, S., Engineered nanoparticles for biomolecular imaging. *Nanoscale* **2011**, 3, (8), 3007-26.
7. Sharma, P.; Singh, A.; Brown, S. C.; Bengtsson, N.; Walter, G. A.; Grobmyer, S. R.; Iwakuma, N.; Santra, S.; Scott, E. W.; Moudgil, B. M., Multimodal nanoparticulate bioimaging contrast agents. *Methods Mol Biol* **2010**, 624, 67-81.
8. Torchilin, V. P., Multifunctional nanocarriers. *Advanced Drug Delivery Reviews* **2006**, 58, (14), 1532-1555.
9. Brigger, I.; Dubernet, C.; Couvreur, P., Nanoparticles in cancer therapy and diagnosis. *Advanced Drug Delivery Reviews* **2002**, 54, (5), 631-651.
10. Ferrari, M., Cancer nanotechnology: opportunities and challenges. *Nat Rev Cancer* **2005**, 5, (3), 161-171.
11. Liu, Z.; Pu, F.; Huang, S.; Yuan, Q.; Ren, J.; Qu, X., Long-circulating Gd(2)O(3):Yb(3+), Er(3+) up-conversion nanoprobes as high-performance contrast agents for multi-modality imaging. *Biomaterials* **2013**, 34, (6), 1712-21.
12. Liu, Z.; Liu, X.; Yuan, Q.; Dong, K.; Jiang, L.; Li, Z.; Ren, J.; Qu, X., Hybrid mesoporous gadolinium oxide nanorods: a platform for multimodal imaging and enhanced insoluble anticancer drug delivery with low systemic toxicity. *Journal of Materials Chemistry* **2012**, 22, (30), 14982-14990.
13. Liu, Z.; Pu, F.; Liu, J.; Jiang, L.; Yuan, Q.; Li, Z.; Ren, J.; Qu, X., PEGylated hybrid ytterbia nanoparticles as high-performance diagnostic probes for in vivo magnetic resonance and X-ray computed tomography imaging with low systemic toxicity. *Nanoscale* **2013**, 5, (10), 4252-61.
14. Kim, D.; Yu, M. K.; Lee, T. S.; Park, J. J.; Jeong, Y. Y.; Jon, S., Amphiphilic polymer-coated hybrid nanoparticles as CT/MRI dual contrast agents. *Nanotechnology* **2011**, 22, (15), 155101.
15. Alric, C.; Taleb, J.; Le Duc, G.; Mandon, C.; Billotey, C.; Le Meur-Herland, A.; Brochard, T.; Vocanson, F.; Janier, M.; Perriat, P.; Roux, S.; Tillement, O., Gadolinium chelate coated gold nanoparticles as contrast agents for both X-ray computed tomography and magnetic resonance imaging. *J Am Chem Soc* **2008**, 130, (18), 5908-15.
16. Santra, S.; Bagwe, R. P.; Dutta, D.; Stanley, J. T.; Walter, G. A.; Tan, W.; Moudgil, B. M.; Mericle, R. A., Synthesis and Characterization of Fluorescent, Radio-Opaque, and Paramagnetic Silica Nanoparticles for Multimodal Bioimaging Applications. *Advanced Materials* **2005**, 17, (18), 2165-2169.

17. Kissell, K. R.; Hartman, K. B.; Van der Heide, P. A.; Wilson, L. J., Preparation of I2@SWNTs: synthesis and spectroscopic characterization of I2-loaded SWNTs. *J Phys Chem B* **2006**, 110, (35), 17425-9.
18. Ananta, J. S.; Godin, B.; Sethi, R.; Moriggi, L.; Liu, X.; Serda, R. E.; Krishnamurthy, R.; Muthupillai, R.; Bolskar, R. D.; Helm, L.; Ferrari, M.; Wilson, L. J.; Decuzzi, P., Geometrical confinement of gadolinium-based contrast agents in nanoporous particles enhances T1 contrast. *Nat Nanotechnol* **2010**, 5, (11), 815-21.
19. Sitharaman, B.; Jacobson, B. D.; Wadghiri, Y. Z.; Bryant, H.; Frank, J., The magnetic, relaxometric, and optical properties of gadolinium-catalyzed single walled carbon nanotubes. *J Appl Phys* **2013**, 113, (13), 134308.
20. Lalwani, G.; Sitharaman, B., Multifunctional Fullerene- and Metallofullerene-based Nanomaterials. *Nano LIFE* **2013**, 03, (03), 1342003.
21. Stankovich, S.; Dikin, D.; Piner, R.; Kohlhaas, K.; Kleinhammes, A.; Jia, Y.; Wu, Y.; Nguyen, S.; Ruoff, R., Synthesis of graphene-based nanosheets via chemical reduction of exfoliated graphite oxide. *Carbon* **2007**, 45, (7), 1558-1565.
22. Sun, X.; Liu, Z.; Welsher, K.; Robinson, J. T.; Goodwin, A.; Zaric, S.; Dai, H., Nano-Graphene Oxide for Cellular Imaging and Drug Delivery. *Nano Res* **2008**, 1, (3), 203-212.
23. Feng, L.; Zhang, S.; Liu, Z., Graphene based gene transfection. *Nanoscale* **2011**, 3, (3), 1252-7.
24. Lalwani, G.; Henslee, A. M.; Farshid, B.; Lin, L.; Kasper, F. K.; Qin, Y. X.; Mikos, A. G.; Sitharaman, B., Two-dimensional nanostructure-reinforced biodegradable polymeric nanocomposites for bone tissue engineering. *Biomacromolecules* **2013**, 14, (3), 900-9.
25. Crowder, S. W.; Prasai, D.; Rath, R.; Balikov, D. A.; Bae, H.; Bolotin, K. I.; Sung, H. J., Three-dimensional graphene foams promote osteogenic differentiation of human mesenchymal stem cells. *Nanoscale* **2013**, 5, (10), 4171-6.
26. Lalwani, G.; Kwaczala, A. T.; Kanakia, S.; Patel, S. C.; Judex, S.; Sitharaman, B., Fabrication and Characterization of Three-Dimensional Macroscopic All-Carbon Scaffolds. *Carbon N Y* **2013**, 53, 90-100.
27. Yang, K.; Hu, L.; Ma, X.; Ye, S.; Cheng, L.; Shi, X.; Li, C.; Li, Y.; Liu, Z., Multimodal imaging guided photothermal therapy using functionalized graphene nanosheets anchored with magnetic nanoparticles. *Adv Mater* **2012**, 24, (14), 1868-72.
28. Shi, X.; Gong, H.; Li, Y.; Wang, C.; Cheng, L.; Liu, Z., Graphene-based magnetic plasmonic nanocomposite for dual bioimaging and photothermal therapy. *Biomaterials* **2013**, 34, (20), 4786-93.
29. Lalwani, G.; Cai, X.; Nie, L.; Wang, L. V.; Sitharaman, B., Graphene-based contrast agents for photoacoustic and thermoacoustic tomography. *Photoacoustics* **2013**, 1, (3-4), 62-67.
30. Kanakia, S.; Toussaint, J. D.; Chowdhury, S. M.; Lalwani, G.; Tembulkar, T.; Button, T.; Shroyer, K. R.; Moore, W.; Sitharaman, B., Physicochemical characterization of a novel graphene-based magnetic resonance imaging contrast agent. *Int J Nanomedicine* **2013**, 8, 2821-33.
31. Paratala, B. S.; Jacobson, B. D.; Kanakia, S.; Francis, L. D.; Sitharaman, B., Physicochemical characterization, and relaxometry studies of micro-graphite oxide, graphene nanoplatelets, and nanoribbons. *PLoS One* **2012**, 7, (6), e38185.
32. Lalwani, G.; Henslee, A. M.; Farshid, B.; Parmar, P.; Lin, L.; Qin, Y. X.; Kasper, F. K.; Mikos, A. G.; Sitharaman, B., Tungsten disulfide nanotubes reinforced biodegradable polymers for bone tissue engineering. *Acta Biomater* **2013**, 9, (9), 8365-73.
33. Lalancette, R. A.; Lukaszewski, D. M.; Steyermark, A., Determination of iodine in organic compounds employing oxygen flask combustion and mercurimetric titration. *Microchemical Journal* **1972**, 17, (6), 665-669.
34. Ferrari, A. C.; Meyer, J. C.; Scardaci, V.; Casiraghi, C.; Lazzeri, M.; Mauri, F.; Piscanec, S.; Jiang, D.; Novoselov, K. S.; Roth, S.; Geim, A. K., Raman Spectrum of Graphene and Graphene Layers. *Physical Review Letters* **2006**, 97, (18), 187401.

35. Dresselhaus, M. S.; Dresselhaus, G.; Saito, R.; Jorio, A., Raman spectroscopy of carbon nanotubes. *Physics Reports* **2005**, 409, (2), 47-99.
36. Shen, J.; Hu, Y.; Shi, M.; Lu, X.; Qin, C.; Li, C.; Ye, M., Fast and Facile Preparation of Graphene Oxide and Reduced Graphene Oxide Nanoplatelets. *Chemistry of Materials* **2009**, 21, (15), 3514-3520.
37. Yao, Z.; Nie, H.; Yang, Z.; Zhou, X.; Liu, Z.; Huang, S., Catalyst-free synthesis of iodine-doped graphene via a facile thermal annealing process and its use for electrocatalytic oxygen reduction in an alkaline medium. *Chem Commun (Camb)* **2012**, 48, (7), 1027-9.
38. Kalita, G.; Wakita, K.; Takahashi, M.; Umeno, M., Iodine doping in solid precursor-based CVD growth graphene film. *Journal of Materials Chemistry* **2011**, 21, (39), 15209-15213.
39. Bagri, A.; Mattevi, C.; Acik, M.; Chabal, Y. J.; Chhowalla, M.; Shenoy, V. B., Structural evolution during the reduction of chemically derived graphene oxide. *Nat Chem* **2010**, 2, (7), 581-7.
40. Ci, L.; Wei, B.; Xu, C.; Liang, J.; Wu, D.; Xie, S.; Zhou, W.; Li, Y.; Liu, Z.; Tang, D., Crystallization behavior of the amorphous carbon nanotubes prepared by the CVD method. *Journal of Crystal Growth* **2001**, 233, (4), 823-828.
41. Endo, M.; Takeuchi, K.; Hiraoka, T.; Furuta, T.; Kasai, T.; Sun, X.; Kiang, C. H.; Dresselhaus, M. S., Stacking nature of graphene layers in carbon nanotubes and nanofibres. *Journal of Physics and Chemistry of Solids* **1997**, 58, (11), 1707-1712.
42. Li, Z. Q.; Lu, C. J.; Xia, Z. P.; Zhou, Y.; Luo, Z., X-ray diffraction patterns of graphite and turbostratic carbon. *Carbon* **2007**, 45, (8), 1686-1695.
43. Lien, H. L.; Zhang, W., Enhanced dehalogenation of halogenated methanes by bimetallic Cu/Al. *Chemosphere* **2002**, 49, (4), 371-8.
44. Fleischmann, M.; Hendra, P. J.; Robinson, J., X-ray diffraction from adsorbed iodine on graphite. *Nature* **1980**, 288, (5787), 152-154.
45. Akhavan, O.; Ghaderi, E.; Akhavan, A., Size-dependent genotoxicity of graphene nanoplatelets in human stem cells. *Biomaterials* **2012**, 33, (32), 8017-25.
46. Mullick Chowdhury, S.; Lalwani, G.; Zhang, K.; Yang, J. Y.; Neville, K.; Sitharaman, B., Cell specific cytotoxicity and uptake of graphene nanoribbons. *Biomaterials* **2013**, 34, (1), 283-93.
47. Mao, H. Y.; Laurent, S.; Chen, W.; Akhavan, O.; Imani, M.; Ashkarran, A. A.; Mahmoudi, M., Graphene: promises, facts, opportunities, and challenges in nanomedicine. *Chem Rev* **2013**, 113, (5), 3407-24.
48. Talukdar, Y.; Rashkow, J.; Lalwani, G.; Sitharaman, B., The Effect of Graphene Nanostructures on Mesenchymal Stem Cells. *Biomaterials* - In Press, 2014.
49. Avti, P. K.; Sitharaman, B., Luminescent single-walled carbon nanotube-sensitized europium nanoprobe for cellular imaging. *Int J Nanomedicine* **2012**, 7, 1953-64.
50. Singh, J.; Daftary, A., Iodinated contrast media and their adverse reactions. *Journal of nuclear medicine technology* **2008**, 36, (2), 69-74.
51. Elmstahl, B.; Nyman, U.; Leander, P.; Chai, C. M.; Golman, K.; Bjork, J.; Almen, T., Gadolinium contrast media are more nephrotoxic than iodine media. The importance of osmolality in direct renal artery injections. *Eur Radiol* **2006**, 16, (12), 2712-20.
52. Worle-Knirsch, J. M.; Pulskamp, K.; Krug, H. F., Oops they did it again! Carbon nanotubes hoax scientists in viability assays. *Nano Lett* **2006**, 6, (6), 1261-8.
53. Xu, C.; Tung, G. A.; Sun, S., Size and Concentration Effect of Gold Nanoparticles on X-ray Attenuation As Measured on Computed Tomography. *Chem Mater* **2008**, 20, (13), 4167-4169.
54. Matsumoto, K.; Jinzaki, M.; Tanami, Y.; Ueno, A.; Yamada, M.; Kuribayashi, S., Virtual monochromatic spectral imaging with fast kilovoltage switching: improved image quality as compared with that obtained with conventional 120-kVp CT. *Radiology* **2011**, 259, (1), 257-62.

55. Rivera, E. J.; Tran, L. A.; Hernández-Rivera, M.; Yoon, D.; Mikos, A. G.; Rusakova, I. A.; Cheong, B. Y.; da Graça Cabreira-Hansen, M.; Willerson, J. T.; Perin, E. C., Bismuth@ US-tubes as a potential contrast agent for X-ray imaging applications. *J. Mater. Chem. B* **2013**, *1*, (37), 4792-4800.
56. Krause, W., Delivery of diagnostic agents in computed tomography. *Adv Drug Deliv Rev* **1999**, *37*, (1-3), 159-173.
57. Rabin, O.; Manuel Perez, J.; Grimm, J.; Wojtkiewicz, G.; Weissleder, R., An X-ray computed tomography imaging agent based on long-circulating bismuth sulphide nanoparticles. *Nat Mater* **2006**, *5*, (2), 118-22.
58. Sitharaman, B.; Wilson, L. J., Gadonanotubes as new high-performance MRI contrast agents. *Int J Nanomedicine* **2006**, *1*, (3), 291-5.
59. Sitharaman, B.; Wilson, L. J., Gadofullerenes and Gadonanotubes: A New Paradigm for High-Performance Magnetic Resonance Imaging Contrast Agent Probes. *Journal of Biomedical Nanotechnology* **2007**, *3*, (4), 342-352.
60. Pan, D.; Caruthers, S. D.; Senpan, A.; Schmieder, A. H.; Wickline, S. A.; Lanza, G. M., Revisiting an old friend: manganese-based MRI contrast agents. *Wiley Interdiscip Rev Nanomed Nanobiotechnol* **2010**.
61. Rohrer, M.; Bauer, H.; Mintorovitch, J.; Requardt, M.; Weinmann, H. J., Comparison of magnetic properties of MRI contrast media solutions at different magnetic field strengths. *Invest Radiol* **2005**, *40*, (11), 715-24.
62. Panich, A.; Shames, A.; Sergeev, N., Paramagnetic Impurities in Graphene Oxide. *Applied Magnetic Resonance* **2013**, *44*, (1-2), 107-116.
63. Panich, A. M.; Shames, A. I.; Aleksenskii, A. E.; Dideikin, A., Magnetic resonance evidence of manganese-graphene complexes in reduced graphene oxide. *Solid State Communications* **2012**, *152*, (6), 466-468.
64. Pei, S.; Cheng, H. M., The reduction of graphene oxide. *Carbon* **2011**.
65. Pei, S.; Zhao, J.; Du, J.; Ren, W.; Cheng, H. M., Direct reduction of graphene oxide films into highly conductive and flexible graphene films by hydrohalic acids. *Carbon* **2010**, *48*, (15), 4466-4474.

Tables:**Table 1:** CD₅₀ values of rGNP-HI against NIH3T3 and A498 cells determined using absorbance-based LDH and fluorescence-based calcein AM assays.

	CD ₅₀ (µg/ml)			
	NIH3T3 cells		A498 cells	
	LDH Assay	Calcein AM	LDH Assay	Calcein AM
rGNP-HI	254	179	301	224

Figure legends:

Figure 1: (A, B) High-resolution TEM images of rGNP-HI depicting multiple layers of graphene nanoplatelets. (C) Low-resolution TEM image depicting a single rGNP-HI. (D) AFM topographical scan of rGNP-HI. (E) AFM height profile showing the thickness of rGNP-HI (F) HRTEM-EDX showing the presence of iodine and manganese. (G, H, I) SEM images of O-GNPs, rGNP-N₂H₂ and r-GNP-HI with the corresponding EDX spectra of the region marked with a red box (inset). (J) SEM-EDX of rGNP-HI reduced using 31.1, 16.05 and 8.02 mM HI.

Figure 2: Raman spectroscopic analysis of (a) pristine graphite, (b) O-GNPs, (c) rGNP-N₂H₂, and (d) rGNP-HI.

Figure 3: Powder x-ray diffraction patterns of (a) pristine graphite, (b) O-GNPs, and (c) rGNP-HI.

Figure 4: Cytotoxicity analysis of rGNP-HI at concentrations ranging from 10-500 µg/ml against NIH3T3 cells and A498 cells after 24 and 48 hours of exposure. (A, B) Percent LDH release (normalized to positive controls, i.e. lysed cells). (C, D) Percentage of cell viability (normalized to positive controls, i.e. cells cultured on TCPS in the absence of rGNP-HI treatment) as measured by quantification of calcein fluorescence. Data are presented as mean ± SD for n = 6 groups. Groups with a significant difference ($p < 0.05$) compared to the TCPS controls at each time point are indicated with ‘*’, and those with a statistical difference between the 24 and 48 hour time points are indicated with ‘#’. (E) Representative fluorescence images of NIH3T3 cells stained with calcein-AM (green) and EthD-1 (red) after 48 hours of exposure to rGNP-HI at 1 µg/ml [(c) & (d)], 10 µg/ml [(e) & (f)], 25 µg/ml [(g) & (h)] and 50 µg/ml [(i) & (j)]. Images (a) & (b) are control cells (no exposure). The size of the scale bars are 100 µm.

Figure 5: (A) CT phantom imaging of DI water, hydroiodic acid, MnCl_2 , and rGNP-HI using a GE 64 slice Lightspeed VCT CT scanner. (B) MRI phantom imaging of hydroiodic acid, MnCl_2 , and rGNP-HI using a GE HTXT 1.5T clinical MRI scanner.

Figures

Figure 1 A:

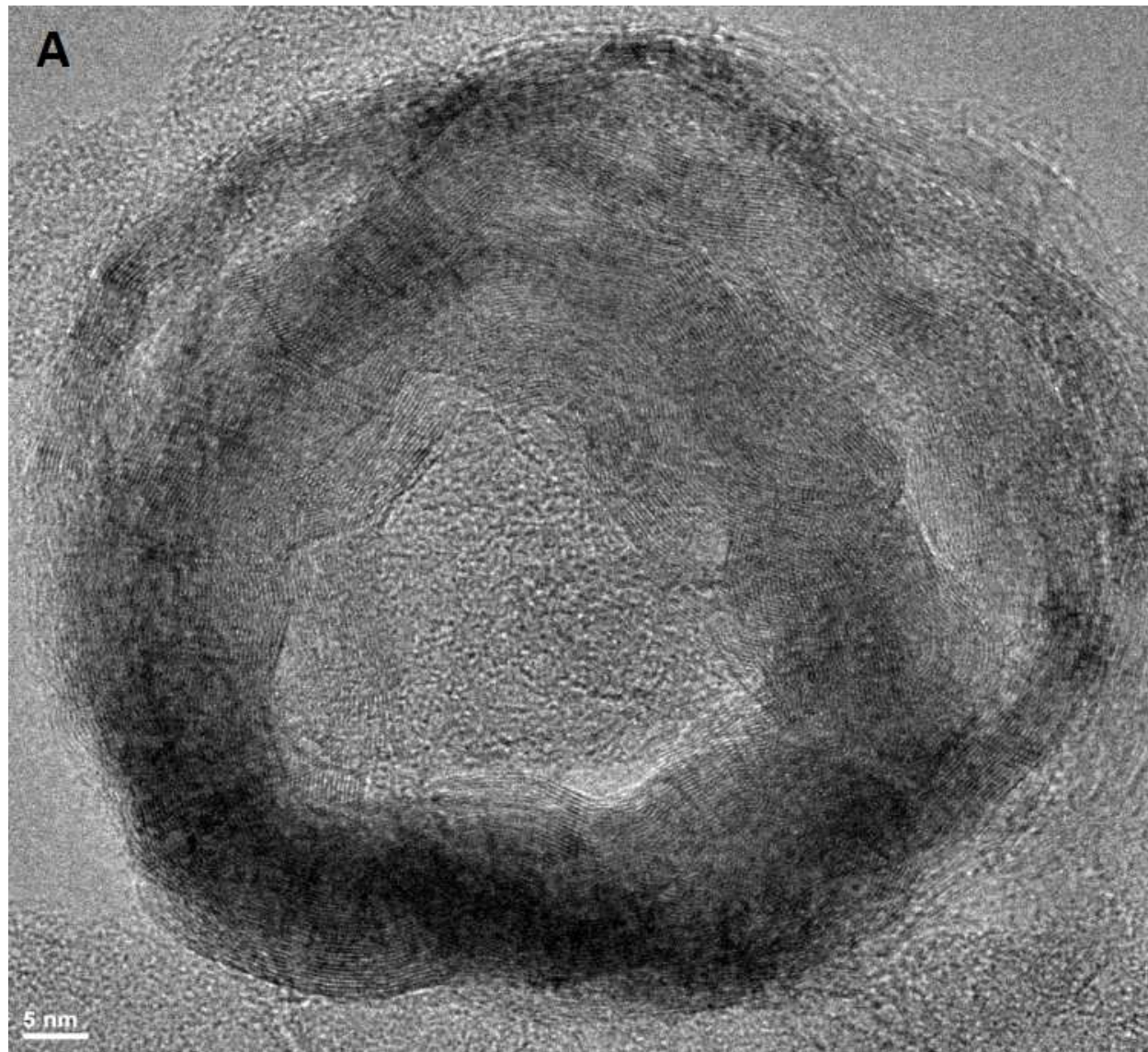


Figure 1 B:

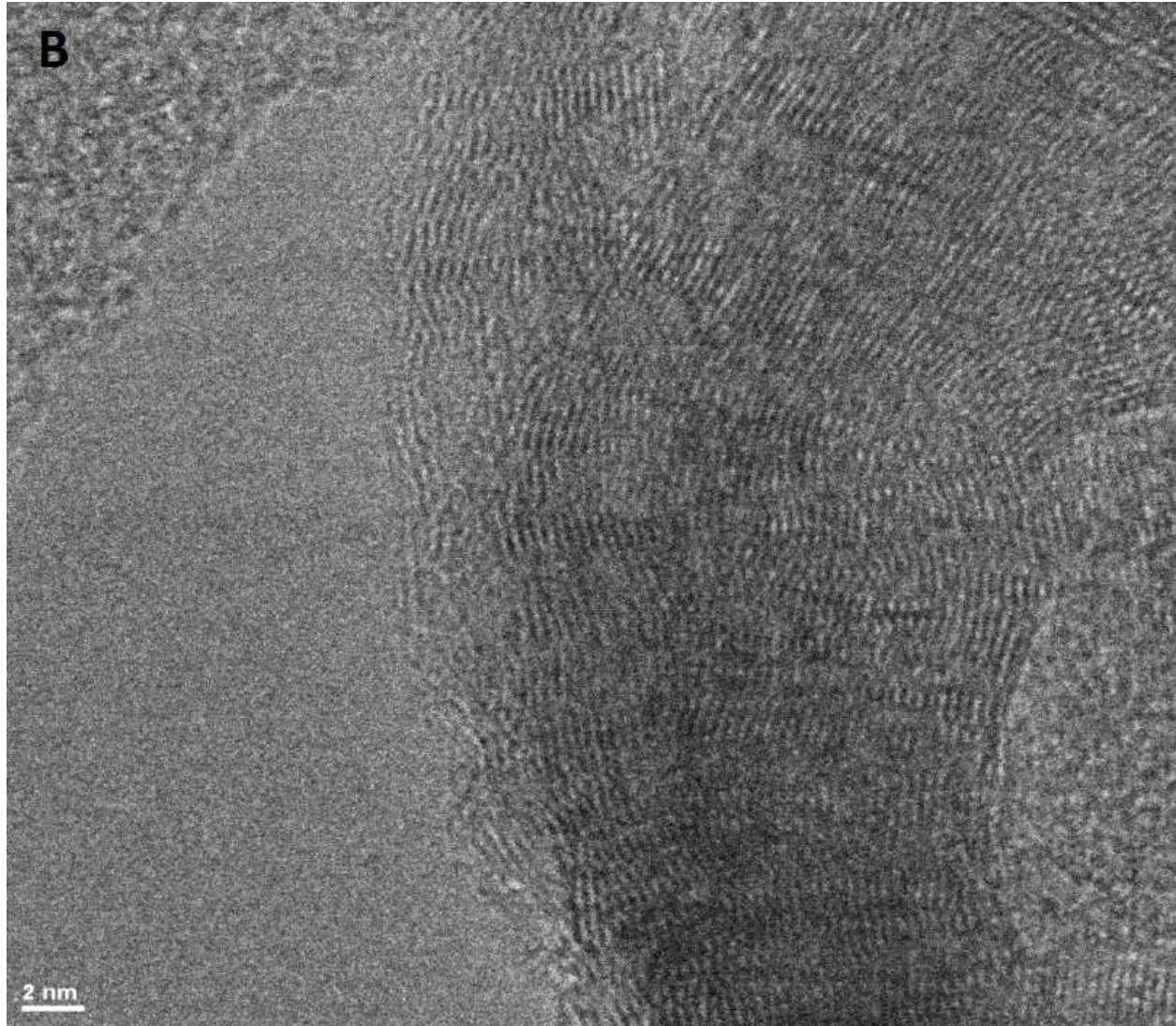


Figure 1 C:

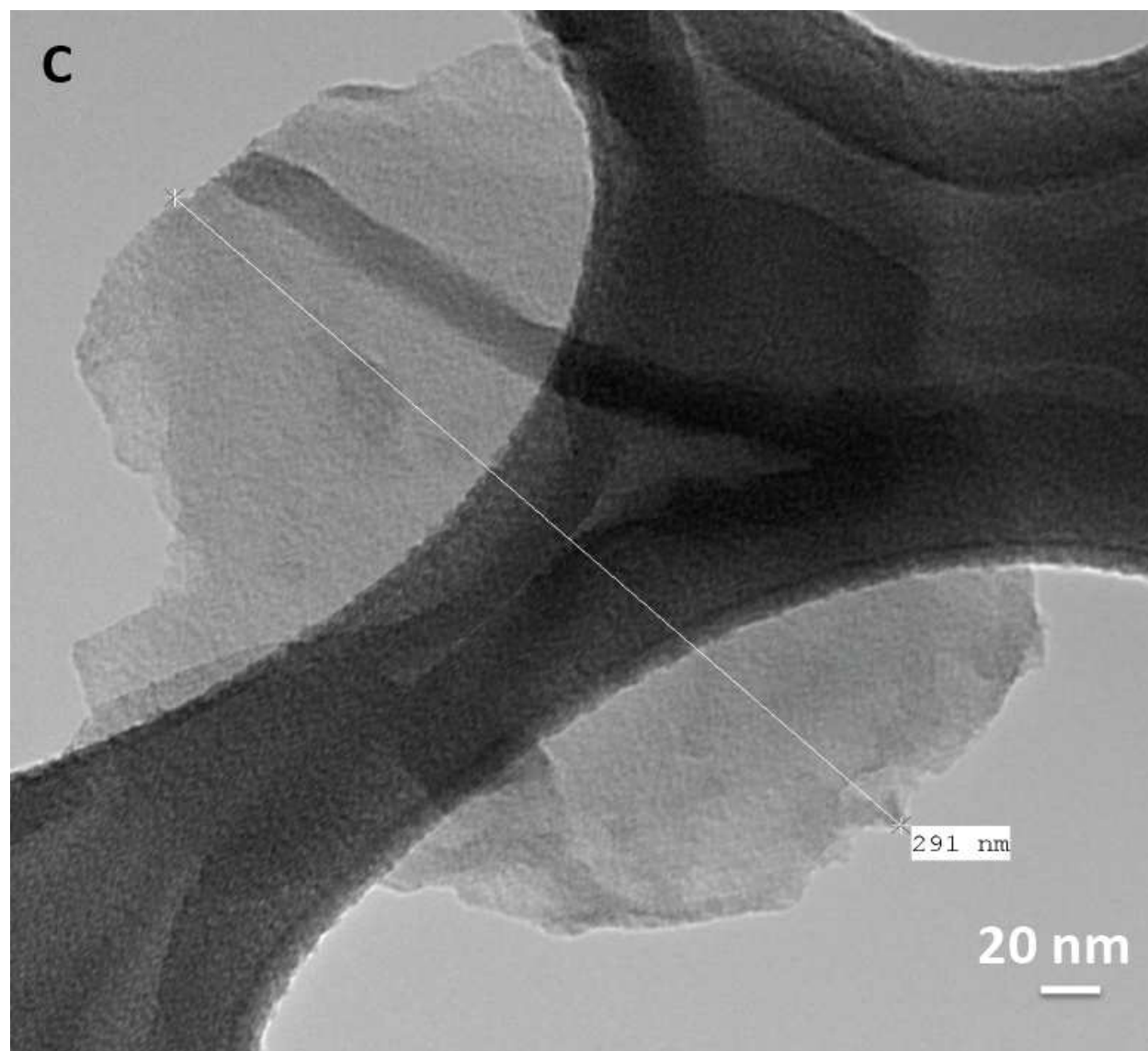


Figure 1 D:

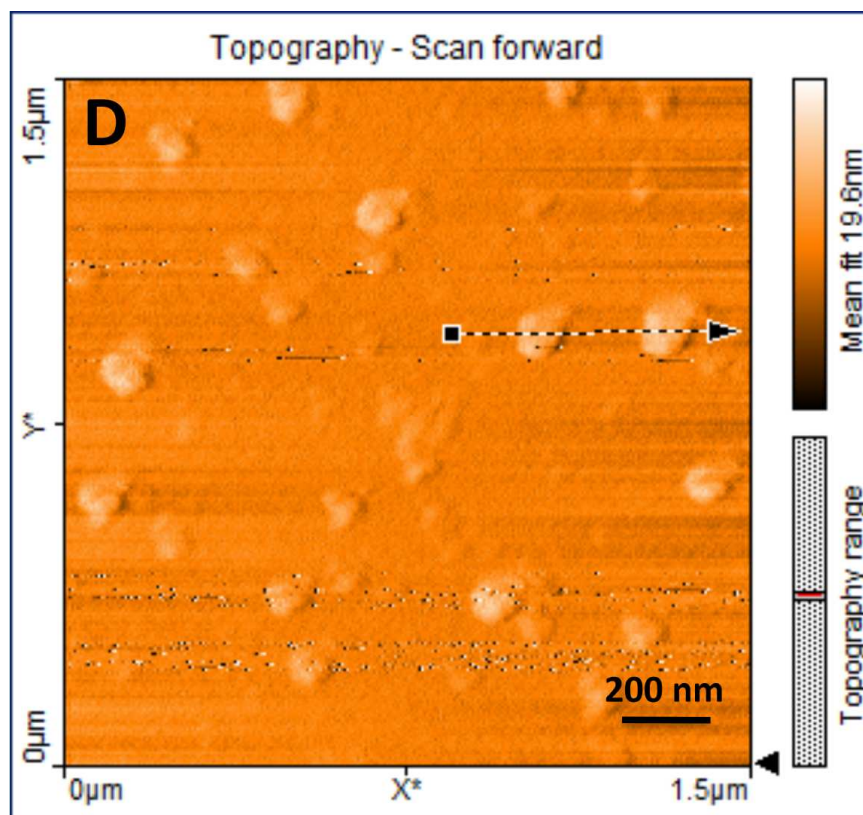


Figure 1 E:

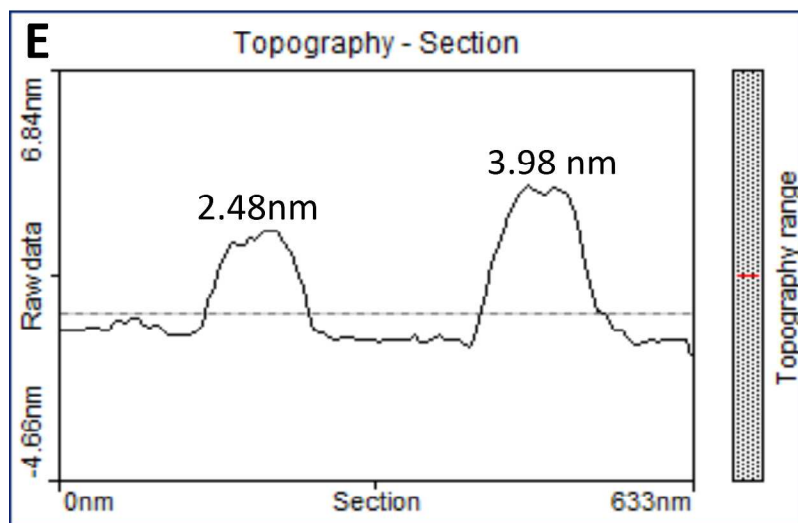


Figure 1 F:

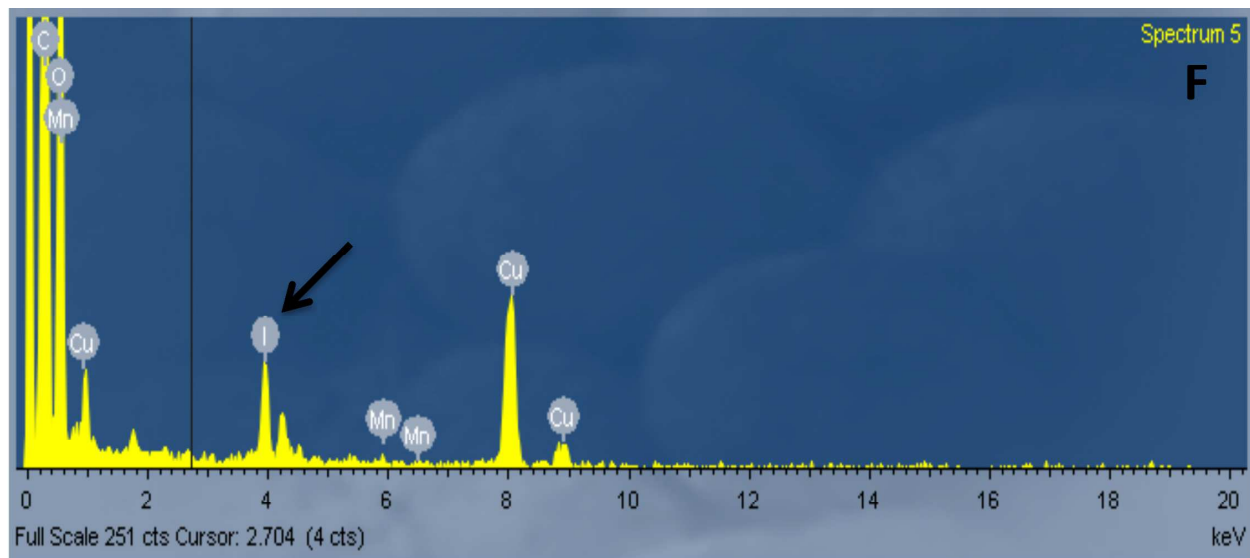


Figure 1 G, H, I:

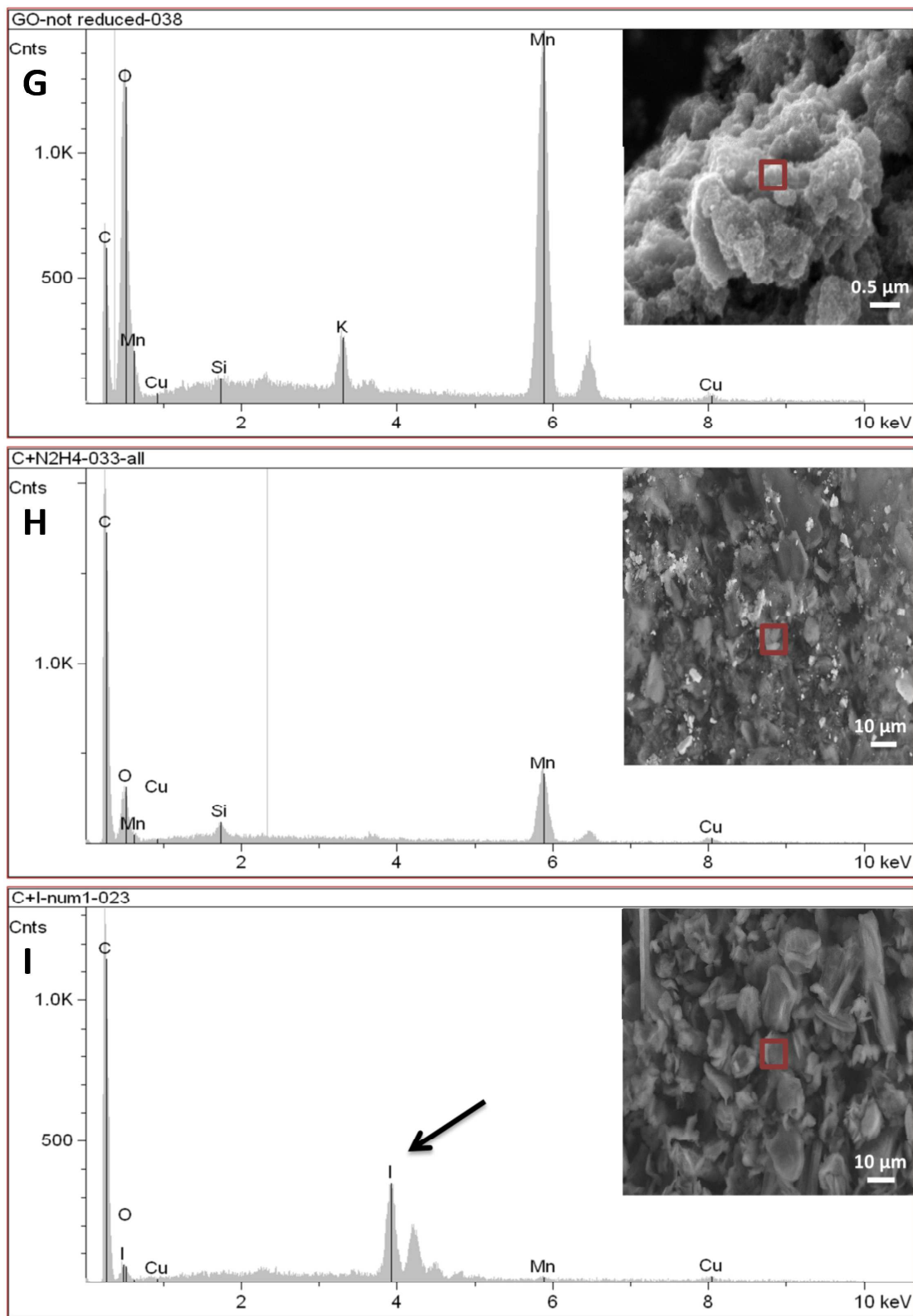


Figure 1 J:

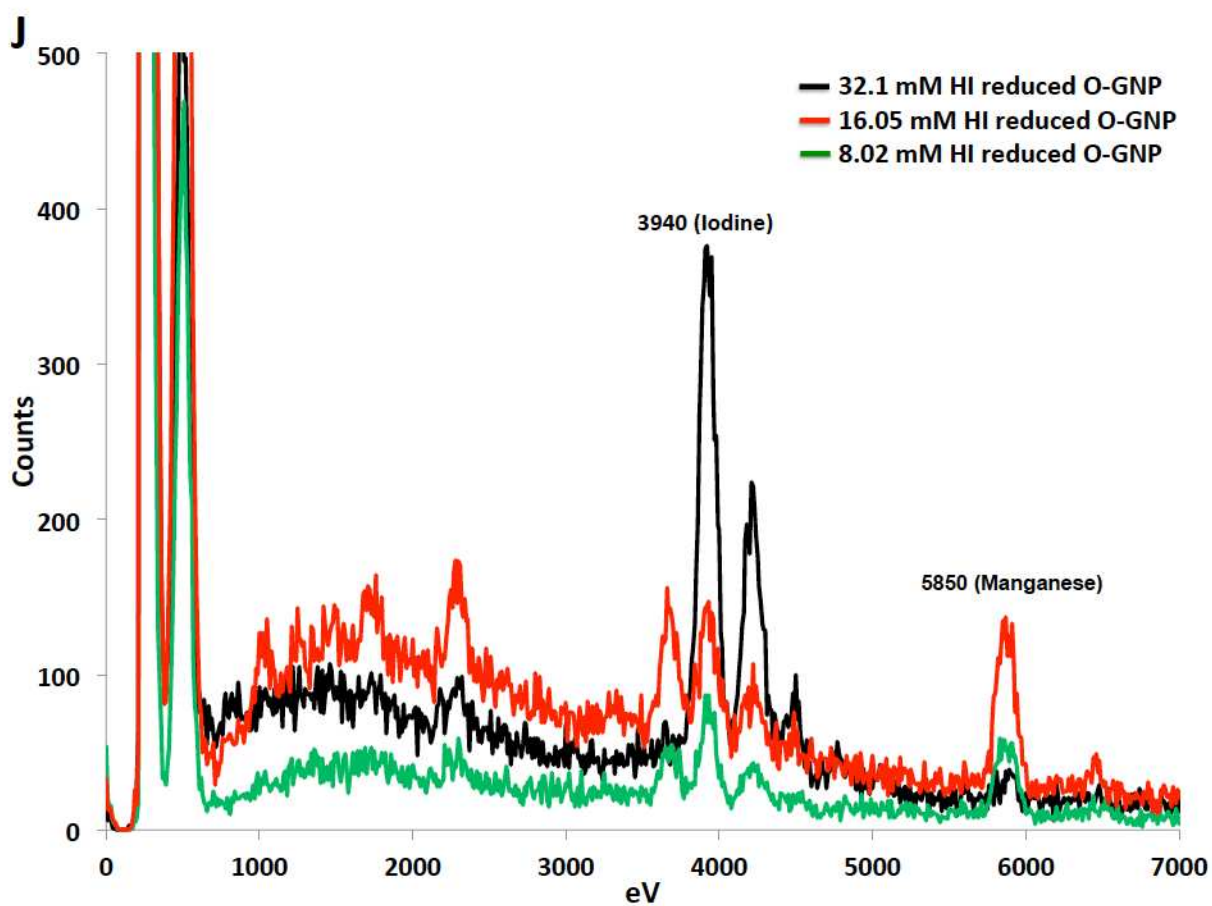


Figure 2:

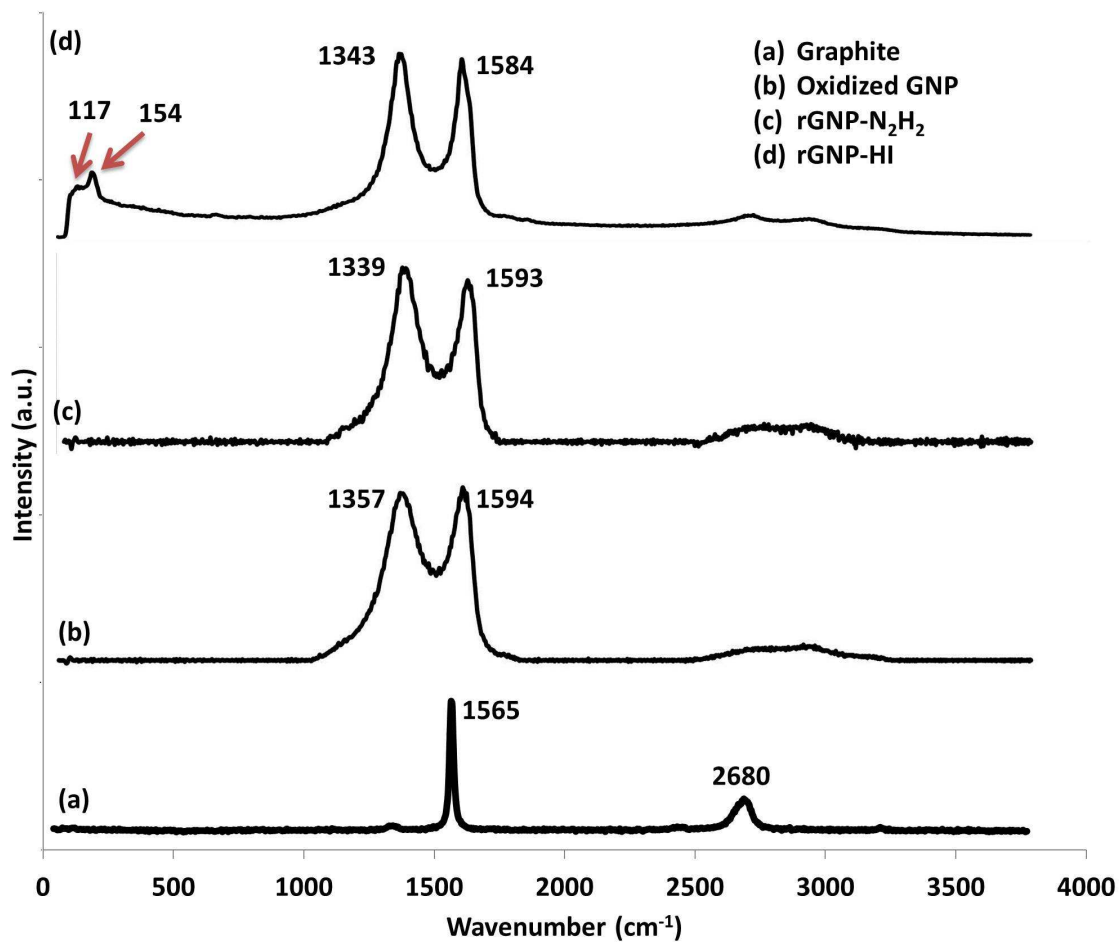


Figure 3:

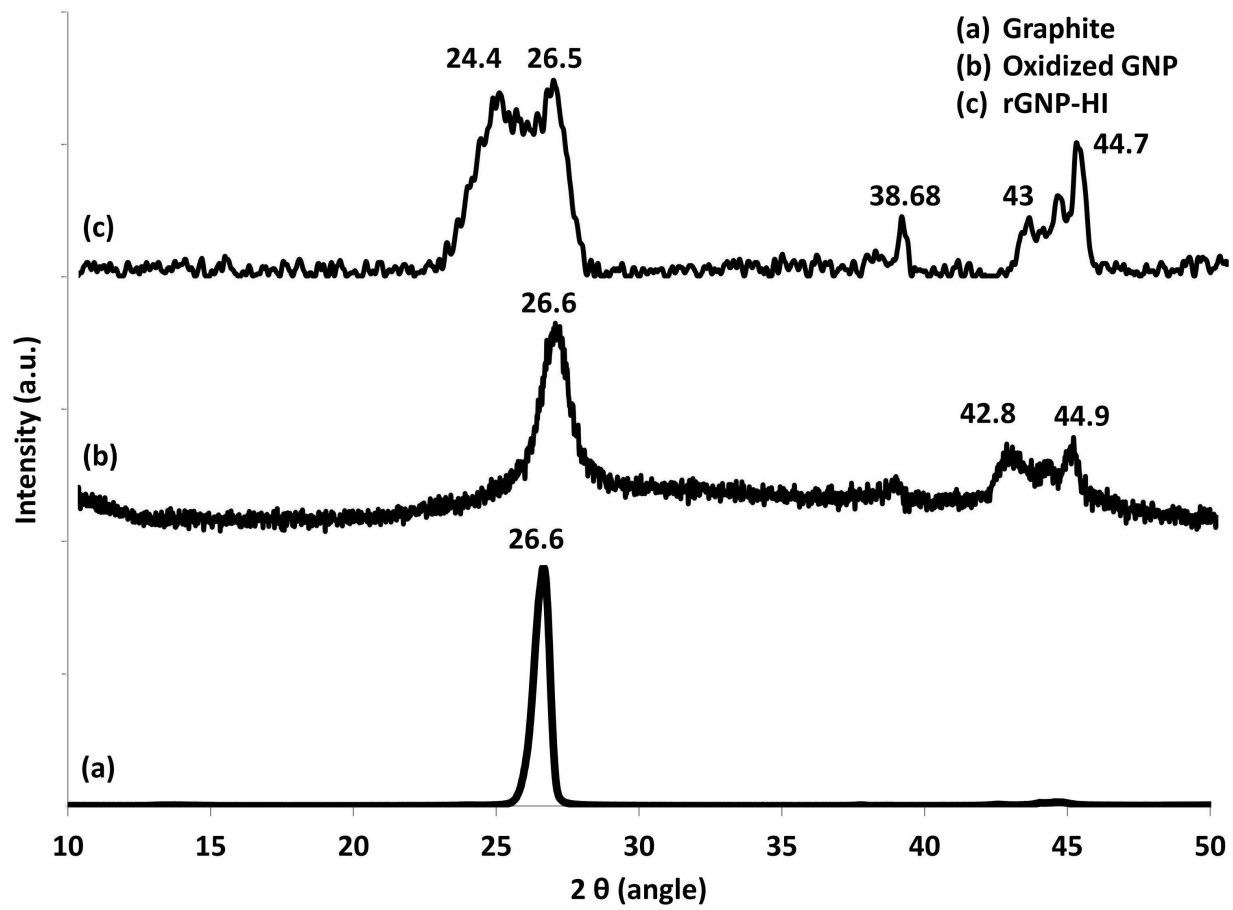


Figure 4 A:

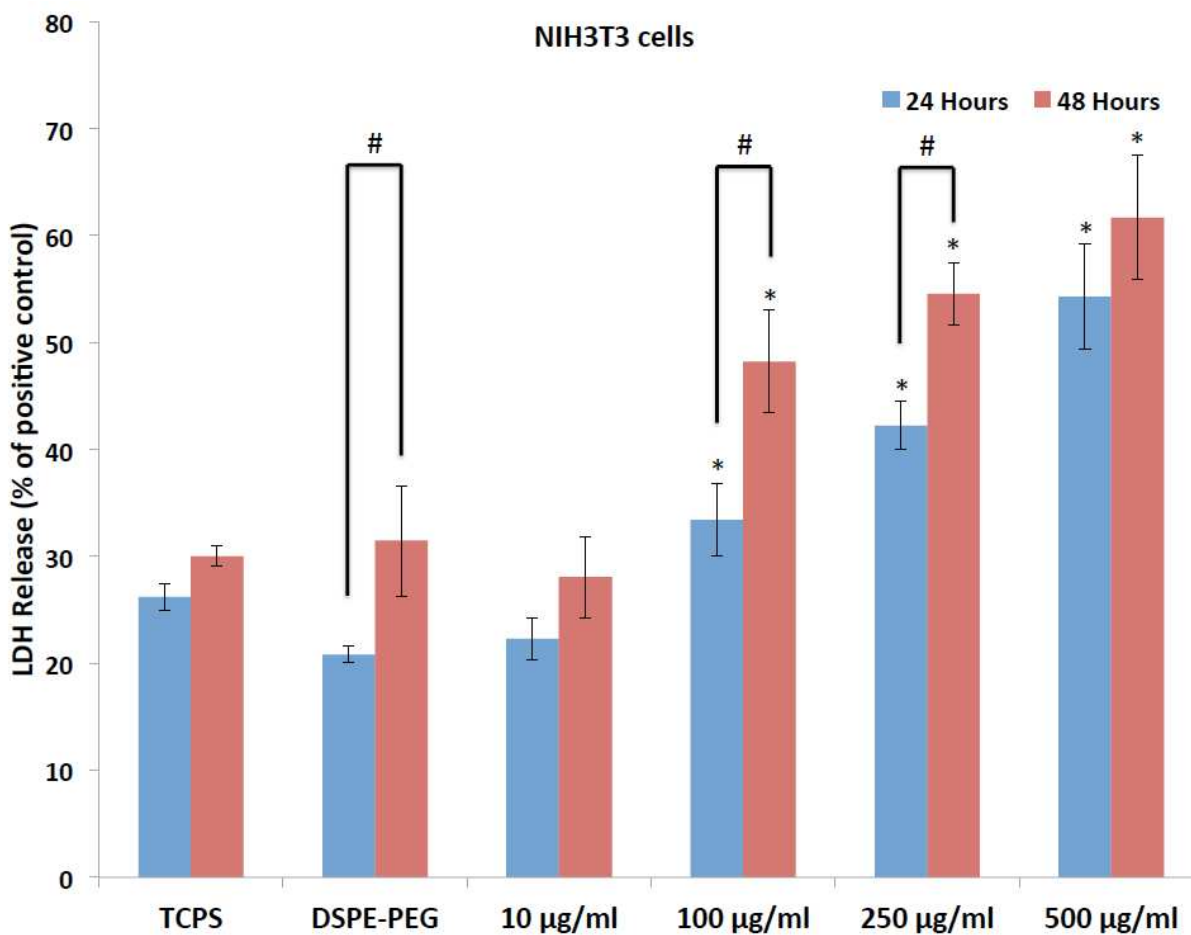


Figure 4 B:

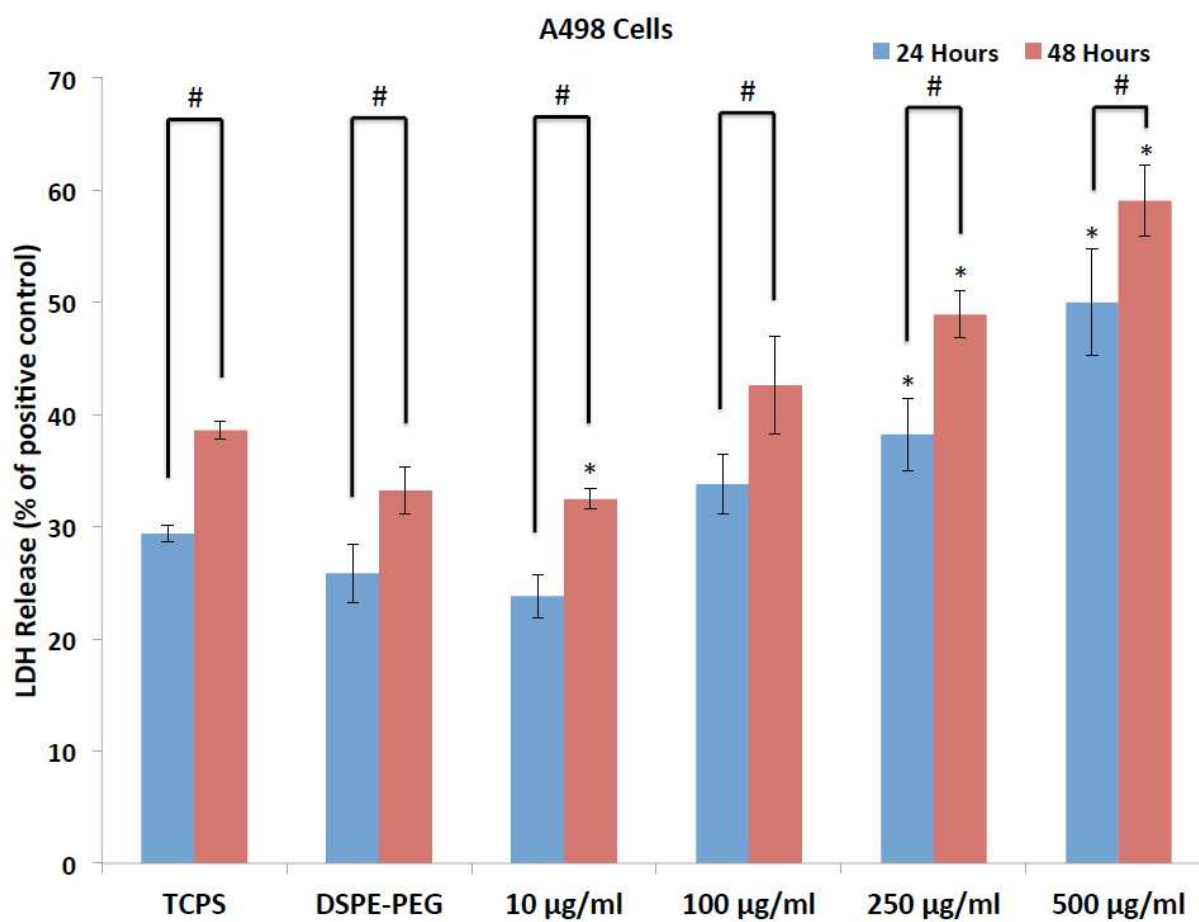


Figure 4 C:

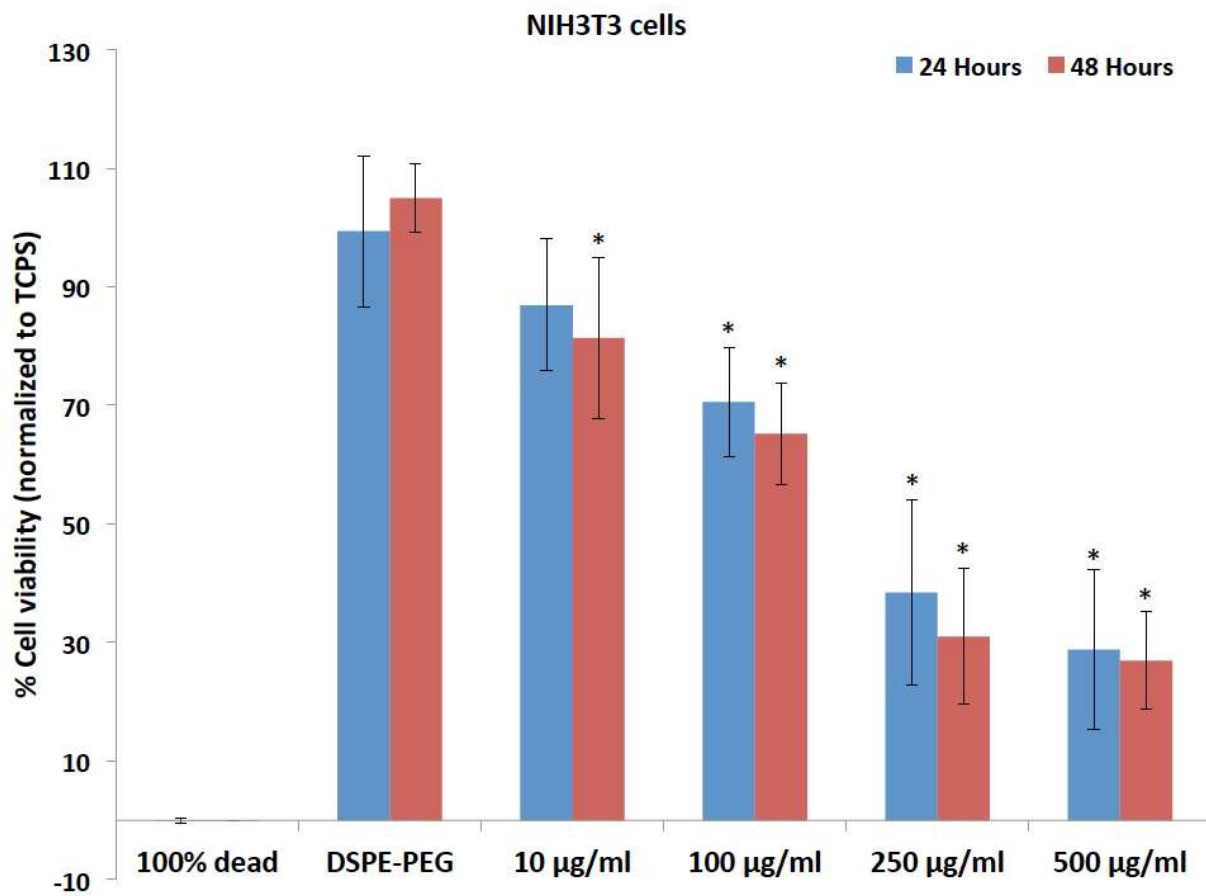


Figure 4 D:

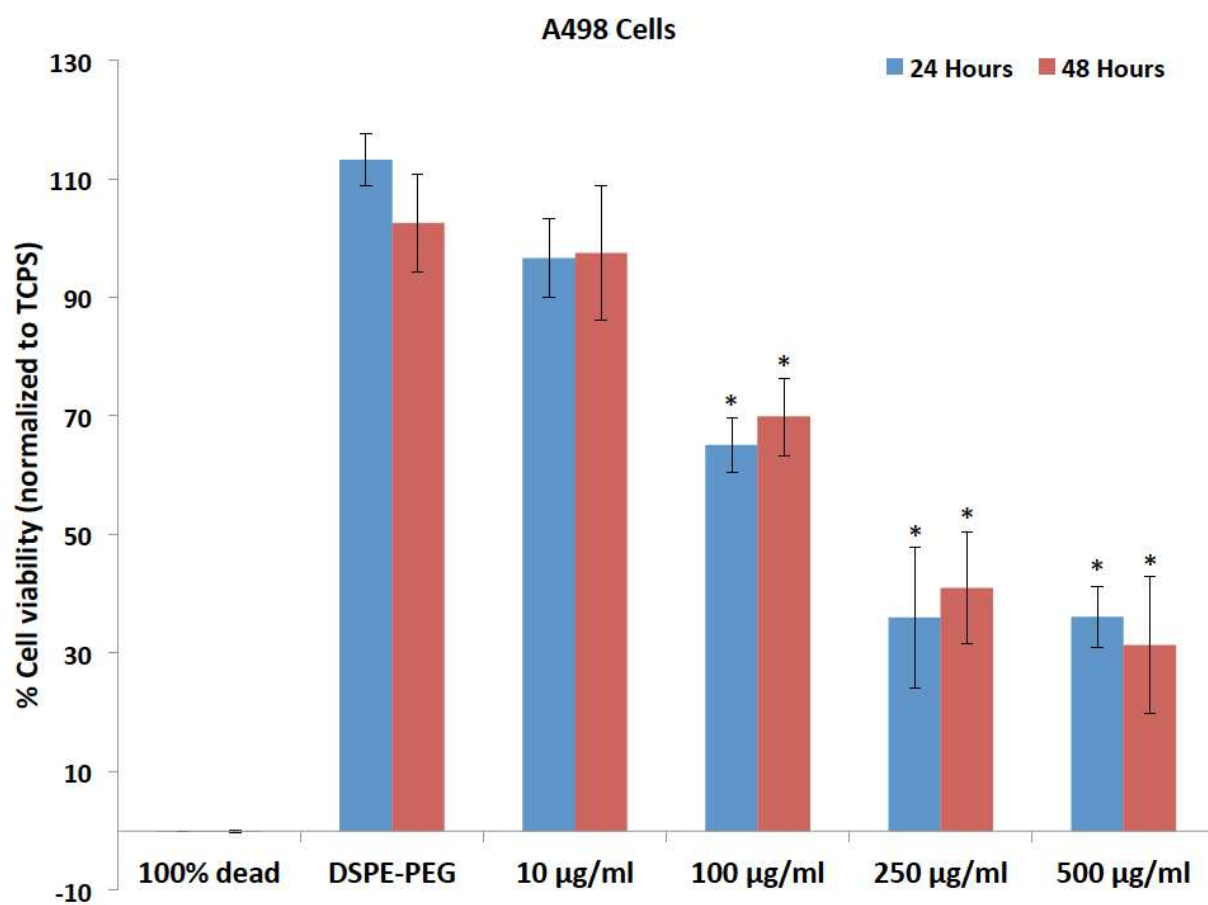


Figure 4 E:

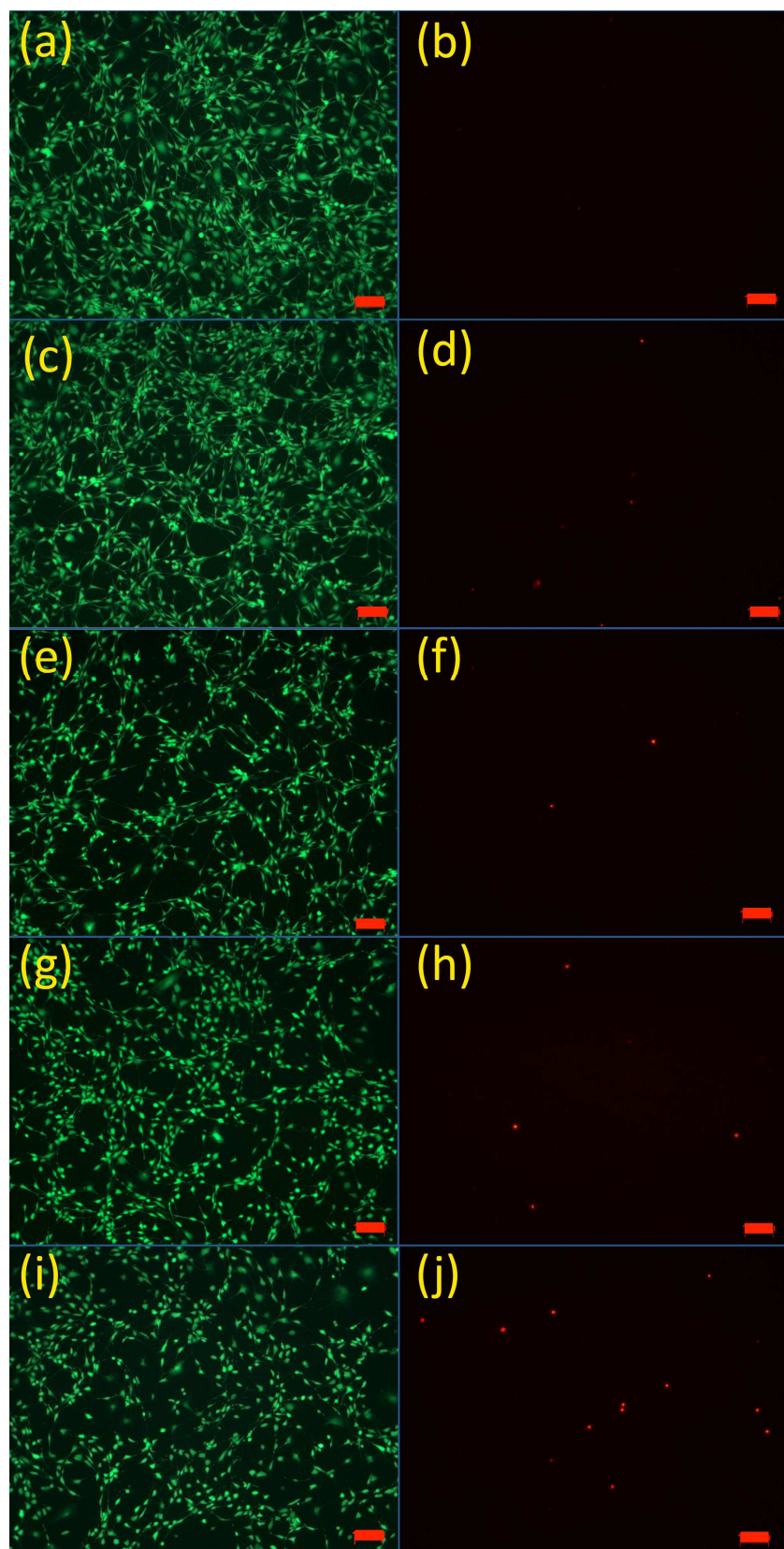


Figure 5 A:

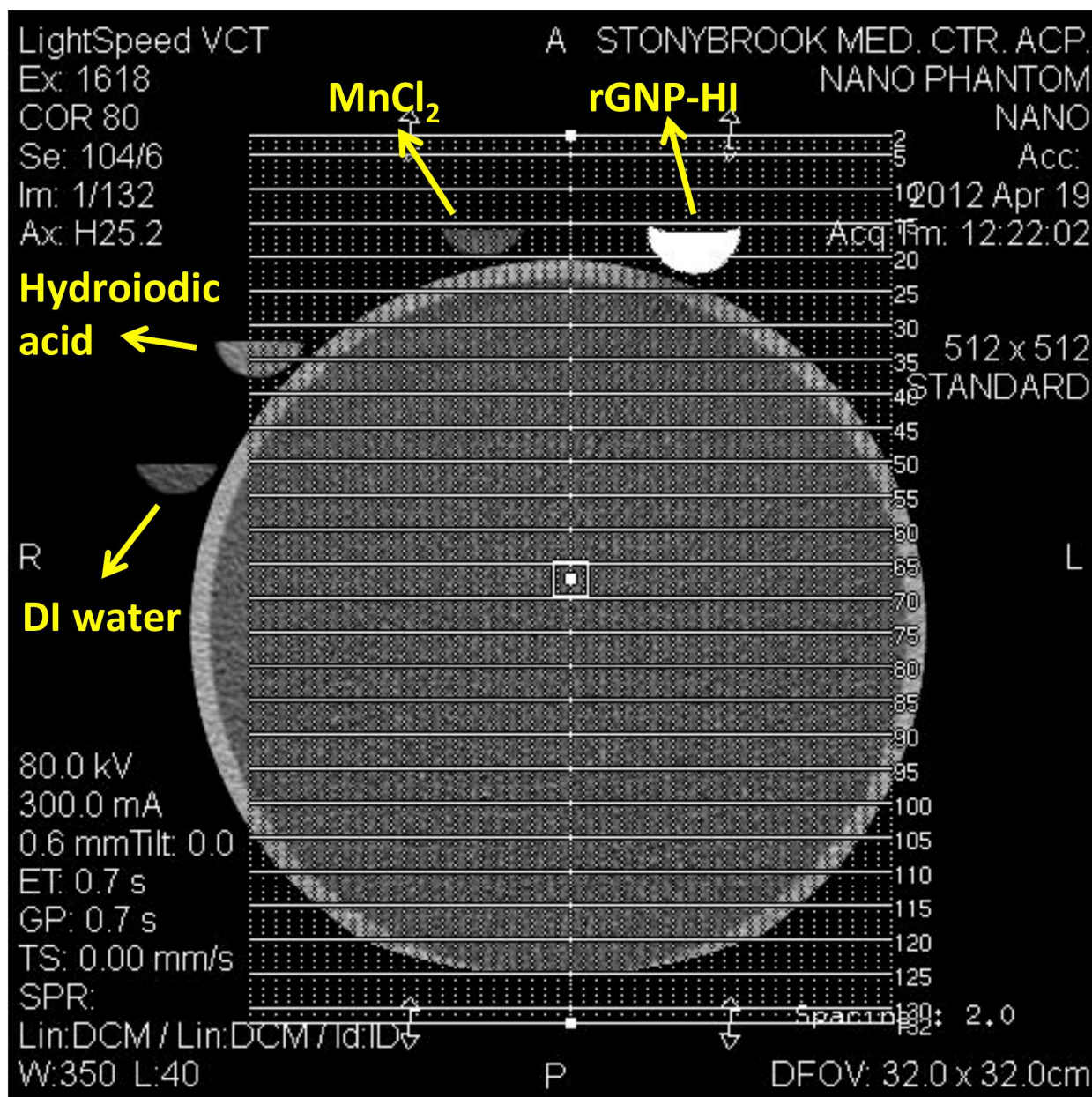


Figure 5 B:

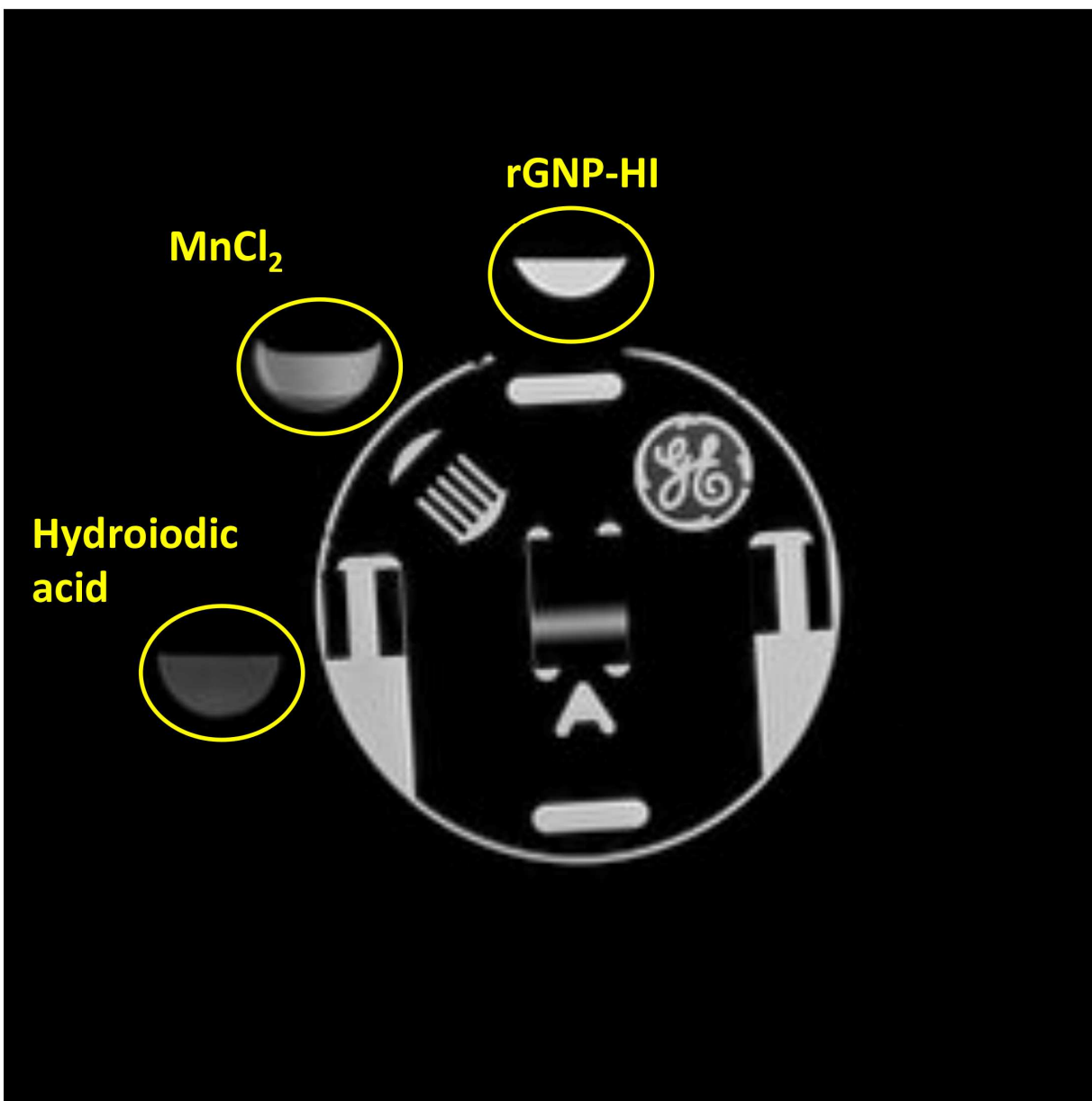


Table of Contents Graphic

Caption: Development of a novel graphene-based multimodal MRI-CT contrast agent

Figure (high-resolution version submitted separately):

